Global drivers of forest loss at 1 km resolution

Michelle Sims[1], Radost Stanimirova[1], Anton Raichuk[2], Maxim Neumann[2], Jessica Richter[1], Forrest Follett[3], James MacCarthy[1], Kristine Lister[1], Christopher Randle[3], Lindsey Sloat[1], Elena Esipova[1], Jaelah Jupiter[1], Charlotte Stanton[4], Dan Morris[4], Christy Melhart Slay[3], Drew Purves[2], Nancy Harris[1]

E-mail: `michelle.sims@wri.org`
[1] World Resources Institute, Washington DC, 20002, USA
[2] Google DeepMind, Zurich, 8002, Switzerland
[3] The Sustainability Consortium, Arizona State University, Tempe, AZ 85281, USA
[4] Google Research, Mountain View, CA 94043, USA

Global drivers of forest loss at 1 km resolution

Michelle Sims[1], Radost Stanimirova[1], Anton Raichuk[2], Maxim Neumann[2], Jessica Richter[1], Forrest Follett[3], James MacCarthy[1], Kristine Lister[1], Christopher Randle[3], Lindsey Sloat[1], Elena Esipova[1], Jaelah Jupiter[1], Charlotte Stanton[4], Dan Morris[4], Christy Melhart Slay[3], Drew Purves[2], Nancy Harris[1]

E-mail: michelle.sims@wri.org
[1] World Resources Institute, Washington DC, 20002, USA
[2] Google DeepMind, Zurich, 8002, Switzerland
[3] The Sustainability Consortium, Arizona State University, Tempe, AZ 85281, USA
[4] Google Research, Mountain View, CA 94043, USA

November 2024

Abstract.

Forests are in decline worldwide due to human activities such as agricultural expansion, urbanization, and mineral extraction. Forest loss due to generally temporary causes, such as wildfire and forest management, is important to distinguish from permanent land use conversion due to the differing ecological and climate impacts of these disturbances and for the purposes of developing effective policies and management strategies. Existing global maps of the drivers of forest loss that are widely used are not spatially or thematically detailed enough for decision makers at local-to-regional scales, such as governments, land managers, or companies. Using publicly available satellite observations (Landsat, Sentinel) and ancillary biophysical and population data, we developed a 1 km resolution, global map of the dominant drivers of forest loss from 2001 to 2022 with seven classes: permanent agriculture (e.g., commodity crops or pasture), hard commodities (e.g., mining), shifting cultivation, forest management (e.g., logging or wood fiber plantations), settlements and infrastructure, wildfire, and other natural disturbances. We interpreted nearly 7,000 reference samples to train a global neural network model that classifies the driver of forest loss with an overall accuracy of 90.5%. Our results show that permanent agriculture was the leading driver of forest loss globally, representing 35% of loss from 2001 to 2022. The drivers of forest loss vary by region, with the leading driver identified as forest management in Europe, permanent agriculture across the tropics, and wildfire in Russia, the Asian mainland, North America, and Oceania. Our results enable assessment of forest disturbance dynamics from local to global scales and can support tracking progress towards corporate and governmental zero-deforestation commitments, monitoring deforestation risks within jurisdictions and supply chains, and assessment of global biodiversity targets.

1. Introduction

Forest loss and degradation are a substantial source of carbon emissions, a leading cause of biodiversity loss, and can negatively impact local communities [27, 22, 12]. While advances in remote sensing have improved the ability to monitor global forest dynamics, available data on tree cover loss [26] do not differentiate permanent (e.g., deforestation) from temporary (e.g., degradation) tree cover loss. The distinction is crucial because the long-term conversion of forests to other land uses has different — often more severe — carbon and ecological impacts compared to forest degradation, management, and other temporary forest disturbances, whether caused by human activities or natural events [48, 5, 23, 6, 45, 27].

A spatially explicit and up-to-date understanding of the drivers of forest loss is fundamental for decision-makers to design and implement targeted forest conservation interventions [69, 20, 33]. Such information is critical for governments devising policies under international frameworks, such as REDD+ (reducing emissions from deforestation and forest degradation in developing countries) under the United Nations Framework Convention on Climate Change (UNFCCC) [35] or National Biodiversity Strategies and Action Plans (NBSAPs) under the UN Convention on Biological Diversity (CBD) [31]. In addition, it is useful for companies striving to eliminate deforestation from their supply chains and for land managers developing strategies to increase forest resilience to disturbances under climate change.

Recognizing this need, attributing the direct drivers of forest loss is an active area of research. A number of studies have quantified drivers using sample-based assessments [15, 46, 4, 16, 78, 56, 21]. However, these methods are challenging to update frequently and are not operational for users who require wall-to-wall maps. Other recent studies have developed models that use satellite remote sensing data to classify and map drivers, including across the tropics [59] or at regional scales, including Africa [49], Europe [68], and Boreal and Arctic regions of North America [86]. The focus has also been on specific drivers such as fire [80], shifting cultivation [11], cocoa [38], mining [44], soybeans [71], logging [34], and rubber [82]. Other studies have focused on the sub-national or country level [62, 67, 14, 36, 53, 32, 21, 51, 47]. Some of the most novel advancements have been in near real time classification of drivers to enable rapid interventions by governments and forest defenders [70]. Many of these studies have used machine learning models, most commonly random forest models [32, 11, 82, 71, 67, 14, 36, 53, 86, 51, 47]; however, deep learning approaches are increasingly being leveraged [59, 62, 49, 38, 70].

Despite these recent advancements, one of the most widely used products attributing the drivers of forest loss is a global study by [13] from 2018 at a coarse spatial resolution of 10 km. Although recent studies offer advantages with regard to higher spatial resolution or more detailed classes with local relevance, they are limited to a specific region or shorter time frames, impeding their ability to provide insights globally for the 21st century. It is crucial to have a globally consistent product to allow for accurate comparisons across regions and provide a clearer understanding of the dynamics of various drivers

over the last two decades.

The goal of the present work was to create a global map of the dominant drivers of forest loss from 2001-2022 at 1 km spatial resolution. To achieve this goal we developed a deep learning model to classify the drivers of tree cover loss from the Global Forest Change (GFC) product [26] according to seven classes. We collected a set of 6,955 training samples through interpretation of very high resolution satellite imagery and developed a single world-wide customized residual convolutional neural network model (ResNet) using satellite data and ancillary biophysical and population data. Our model classifies the direct driver that caused the majority of tree cover loss area within each 1 km grid cell from 2001-2022. The improvement in thematic and spatial resolution allowed us to differentiate losses that may be temporary in nature (due to logging and wood-fiber harvest, wildfire and other natural disturbances) from deforestation (due to agricultural activities, settlements and infrastructure, and hard commodity expansion).

2. Methods

2.1. Definitions

This study classifies the dominant driver of forest loss from 2001-2022 at 0.01 degree (approximately 1 km at the equator) spatial resolution, globally. Forest loss is defined, following [26], as stand-replacement disturbances that remove woody vegetation exceeding 5 m in height. The "dominant" driver is defined as the direct driver that caused the majority of tree cover loss area as detected by [26] within each 1 km grid cell from 2001-2022. In this study we divide the world into seven regions: North America, Latin America, Europe, Africa, Asia (including East/South/Central Asia & Middle East), Southeast Asia, and Oceania (Figure S1). We map seven driver classes: permanent agriculture, hard commodities, shifting cultivation, forest management, wildfires, settlements and infrastructure, and other natural disturbances (Table 1, Figure 1).

2.2. Training data collection

An initial set of training samples were generated using a global stratified random sample based on the seven driver classes. Samples were collected from the 1 km grid overlaid with tree cover loss data from the GFC product [26]. To avoid sampling noise, we subset the grid cells to those where tree cover loss makes up at least 0.5%.

Training data were interpreted by a team of nine trained image analysts using the drivers of forest loss definitions (Table 1) and a suite of online tools, accessed through the Google Earth Engine API [25]. Image analysts interpreted drivers on-screen using a combination of high-resolution imagery, time series of spectral reflectance and indices, as well as contextual layers (see section S1, Table S3). The 1 km grid cells served as the basic unit of interpretation. For each grid cell (plot), analysts collected information on the primary driver of loss (greater than 50% of the loss within the plot), secondary driver of loss, and their confidence in assigning each label. We had a "Noise" category that

Driver	Definition
Permanent agriculture	Long-term, permanent tree cover loss for small- to large-scale agriculture. This includes perennial tree crops such as oil palm, cacao, orchards, nut trees, and rubber, as well as pasture and seasonal crops and cropping systems, which may include a fallow period.
Hard commodities	Tree cover loss due to the establishment or expansion of mining or energy infrastructure. Mining activities range from small-scale and artisanal mining to large-scale mining. Energy infrastructure includes power lines, power plants, oil drilling and refineries, wind and solar farms, flooding due to the construction of hydroelectric dams, and other types of energy infrastructure.
Shifting cultivation	Tree cover loss due to small- to medium-scale clearing for temporary cultivation that is later abandoned and followed by subsequent regrowth of secondary forest or vegetation.
Forest management	Forest management and logging activities occurring within managed, natural or semi-natural forests and plantations, often with evidence of forest regrowth or planting in subsequent years. This includes harvesting in wood-fiber plantations, clear-cut and selective logging, establishment of logging roads, and other forest management activities such as forest thinning and salvage or sanitation logging.
Wildfire	Tree cover loss due to fire with no visible human conversion or agricultural activity afterward. Fires may be started by natural causes (e.g. lightning) or may be related to human activities (accidental or deliberate).
Settlements and infrastructure	Tree cover loss due to expansion and intensification of roads, settlements, urban areas, or built infrastructure (not associated with other classes).
Other natural disturbances	Tree cover loss due to other non-fire natural disturbances, including storms, flooding, landslides, drought, windthrow, lava flows, sediment flow or meandering rivers, natural flooding, insect outbreaks, etc. If tree cover loss due to natural causes is followed by salvage or sanitation logging, it is classified as forest management.

Table 1. Drivers of forest loss classes used in this study and their definitions

was used when the tree cover loss data by [26] indicated loss but upon interpretation it turned out to be a false positive with no actual loss on the ground (e.g., due to cloud or sensor issues, misclassification, etc.). Each plot was reviewed for quality by a duo of senior analysts with domain expertise, resulting in a total of 5,179 plots globally.

Figure 1. Examples of satellite imagery representing the seven driver classes used in this study. Map data: Google, Maxar Technologies, and Airbus.

We collected 2,607 additional training plots via an active learning workflow to improve classifications (section S1). The initial training dataset and active learning dataset combined resulted in 7,786 plots, of which 831 (11%) were removed due to low confidence (7%) and noise (4%). The resulting final training dataset used in model development had 6,955 plots (Figure S2, Table S1), the majority of which had high confidence (80%). Nearly a quarter (22%) had a secondary driver in addition to a primary driver.

2.3. Model input data and pre-processing

The basis of this model and a core input is the GFC product v1.10 [26], which includes the year of tree cover loss along with first and last Landsat 7 cloud-free composite, updated through 2022, at 1 arc second (approximately 30 m at the equator). The first composite is from the first available year, circa 2000. The last image composite is from 2022 or the closest year with cloud free data.

Additionally, the model included data from Sentinel-2, as well as ancillary biophysical and population data relevant to our driver classes (Table 2). For more information on the input data specifications and pre-processing steps, see section S2. Dataset generation steps were conducted in Google Earth Engine [25], resulting in model input data as presented in Table 2.

Table 2. Model input data description and dimensions ([time], height, width, bands).

Data source	Bands	Dimensions
Global Forest Change [26]	9 bands: tree cover in 2000, tree cover loss, tree cover gain, loss year, data mask, and two Landsat 7 composites (for the year 2000 and 2022) of 4 channels each (red, NIR, SWIR1, SWIR2)	(112, 112, 13)
Sentinel-2	5 bands: peak summer composites for 5 bands (B3, B4, B5, B7, B12) with 10m and 20m resolution channels for three years (2018, 2020, 2022)	(3, 112, 112, 5)
Global Human Settlement Layer (GHSL) Global population surfaces [66]	Single band for 7 time intervals (1995, 2000, 2005, 2010, 2015, 2020, 2025 [projected])	(7, 112, 112, 1)
Tree cover loss due to fire [80]	Single binary band indicating fire (1) and not fire (0)	(112, 112, 1)
Mining dataset [50, 17, 75]	Single binary band indicating presence of mining sites (1) and no mining (0), created by taking the union of the input data sources	(112, 112, 1)
Dynamic World [9]	3 bands: annual mean probability for 3 land cover classes (grass, crops, shrub/scrub) for three years (2016, 2019, 2022)	(3, 112, 112, 3)
Copernicus GLO 30 m Digital Elevation Model with forest and building removed (FABDEM) [28]	3 bands: elevation, slope, aspect	(112, 112, 3)
Region annotation	Single value	(1, 1, 1)
Latitude	Single value	(1, 1, 1)
Longitude	Single value	(1, 1, 1)

2.4. Model architecture

Initially, we conducted comparisons with a random forest baseline model and compared it against convolutional [29, 42] and vision transformer [43, 2] based neural network models [61]. A variant of convolutional neural networks called the Residual Network (ResNet) model performed best, so we tuned its architecture to better fit our 1 km resolution geospatial data. We adjusted the first stem layer of the model and reduced the depth of the network while also increasing the width of the layers. This resulted in a model with 12.8 M parameters.

2.5. Training a model ensemble

To tune the model and optimize the parameters, we used a 5-fold cross-validation. The model was trained for 10 epochs with gradient descent using the Adam optimizer with weight decay [41].

For robust evaluation, we used 20 random seeds to initialize the model weights and for training data random augmentation, resulting in total in 100 trained models (5 folds x 20 random seeds). For a full list of the tuned training parameters for the best model configurations, see Table S4. The overall scheme of data flow from model training to global inference map generation is outlined in Figure 2.

Since we had a relatively small number of examples for a deep learning approach, we ensemble a set of trained models to reduce model uncertainty [8]. We constructed an ensemble by varying model depth and width, number of training epochs, and random seeds for model weight initialization. For each 5-folds model training, we selected the best two models based on the evaluation fold to be kept in the ensemble. Additionally, we used the technique of "label smoothing" for some models in the ensemble, which makes the training more robust against potential errors and uncertainties in the training data [74]. See section S3 for more information.

The spatial extent of the inference map is the global area where tree cover loss is detected by the GFC product [26], excluding areas where tree cover loss comprised less than 0.5% of the 1 km grid cell, due to the challenges of making accurate predictions on these small areas of loss. In addition to the driver of forest loss classification, we produced maps of the probability of each class (section 7).
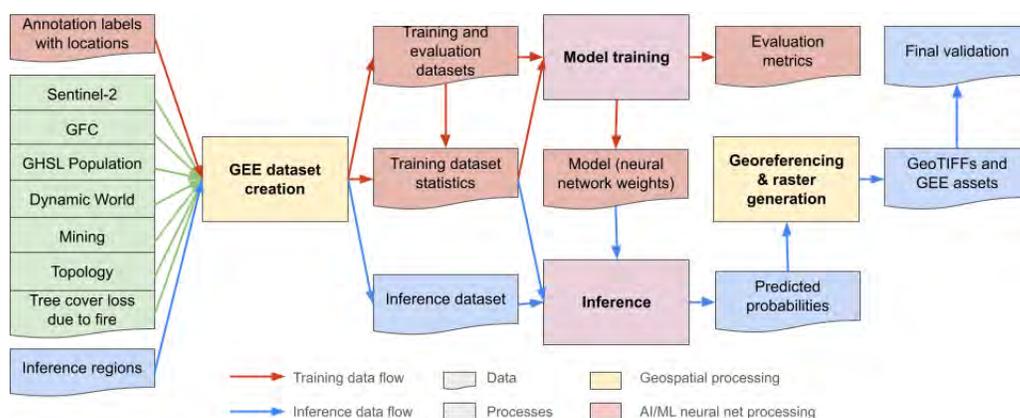
Figure 2. Diagram illustrating the overall flow of data and model training, outlining different flows for model training and inference, and distinguishing geospatial-data specific processing and domain-agnostic machine learning.

2.6. Validation data collection

A stratified random sample of 3,574 1 km plots (Figure S3) was used to estimate the accuracy of the final classification map. We used a similar interpretation protocol for

the validation and training data collection (described in subsection 2.2, section S1). Validation plots were identified and collected independently of training plots following the best practices outlined in [55] and [73]. We stratified our accuracy assessment based on seven regions and seven driver classes for a total of 49 strata. Sample sizes per strata were derived using an initial map version and an optimal sample allocation based on guidance in [55].

2.7. Sample-based estimation of driver proportions

The validation sample was used to estimate the proportion of tree cover loss from 2001-2022 [26] attributable to each driver in each of the seven regions and globally. The number of plots randomly selected from each stratum are shown in Table S2. We used a ratio estimator as described by [72] and [13]. We weighted the results by the area of tree cover loss such that plots with more tree cover loss were weighted higher as per [13]. We calculated the overall, producer's and user's accuracies, as well as driver proportions with 95% confidence intervals using the validation plots (Table S5, Table 3). Reported results include validation plots labeled as "Noise" (Table S2); accuracies generated with noise-free validation plots were comparable.

2.8. Map-based comparison with prior estimates

We compared the results from our map with the Curtis *et al.* [13] drivers of forest loss map at 10 km resolution, updated through 2022 to match the time period of our study. We calculated the proportion of the total area of tree cover loss from 2001-2022 attributed to each driver by overlaying the GFC tree cover loss data v1.10 [26] with our 1 km drivers map and with the updated Curtis *et al.* drivers map, and summed the area of loss for each driver globally and by region. We combined our permanent agriculture and hard commodities class for the comparison, since these were grouped into a single class (commodity-driven deforestation) in [13]. We compared our settlements & infrastructure class to the urbanization class in Curtis *et al.*, and excluded other natural disturbances from the comparison, since this class was not included in [13].

3. Results
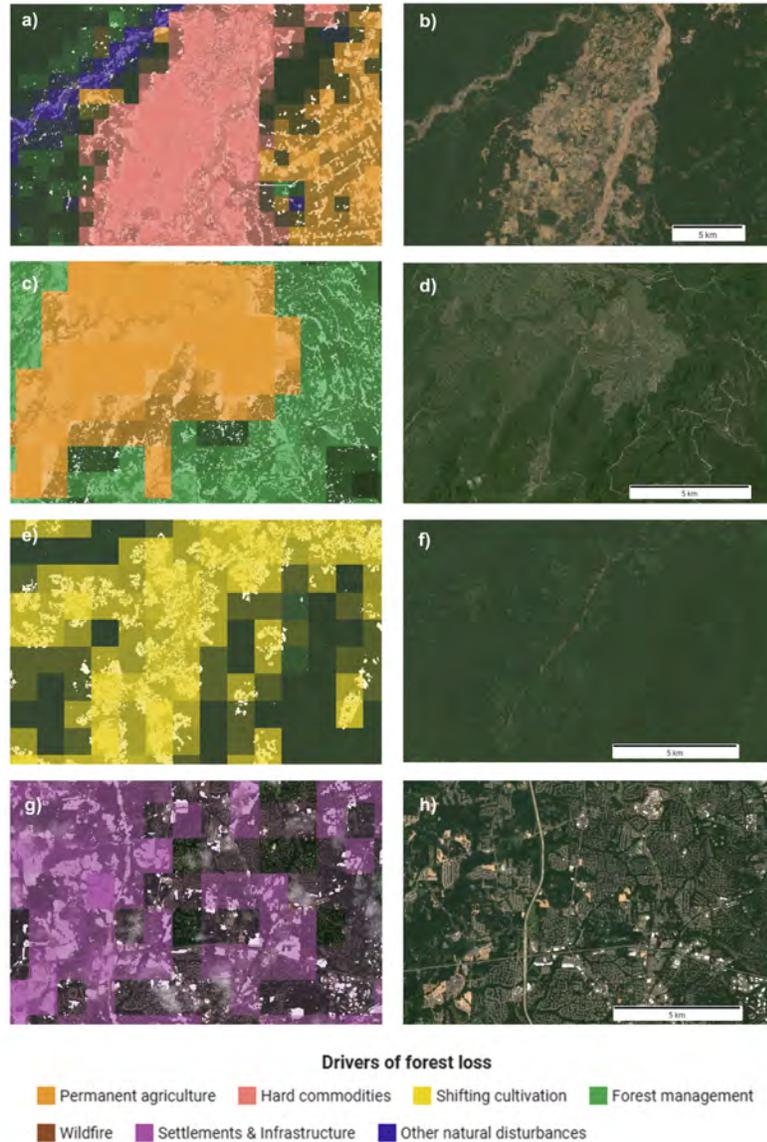
3.1. Global and regional drivers of forest loss

Our results indicate that permanent agriculture was the leading driver of tree cover loss, accounting for 35±3% of loss globally from 2001-2022 (Table 3). Permanent agriculture was predominant in tropical regions (Figure 3), and was attributed to 69±6% of loss in Latin America, 61±7% in Southeast Asia, and 51±7% in Africa. Our model classified loss associated with diverse types of permanent agriculture, ranging from commodity crop production, such as palm oil and rubber in Southeast Asia, pasture and soy in Latin America, and cocoa in West Africa, to small-scale or subsistence agricultural expansion, such as in dry tropical forests in Africa.

The second largest driver of tree cover loss was wildfire, approximately 29±2% of loss globally, followed by forest management at 23±2%. Wildfire and forest management were predominant in temperate and boreal regions. Wildfire represented 65±5% and 66±5% of loss in Asia and Oceania, respectively, and 45±6% in North America. In Asia, the majority of wildfire-driven loss occurred in Russia. Forest management accounted for the majority of tree cover loss in Europe (85±4%) and nearly half of all loss in North America (45±6%). Our model classified large areas of selective logging in the tropics, with higher spatial resolution relative to previous studies [13], allowing for delineation of these disturbances when they co-occur with other land uses, such as agriculture (Figure 4).

Globally, 8±1% of tree cover loss was attributed to shifting cultivation, primarily in Africa and Southeast Asia, with a smaller proportion in Latin America. Shifting cultivation represented 37±6% of tree cover loss in Africa, 11±4% in Southeast Asia, and 4±2% in Latin America. Hard commodities, other natural disturbances, and expansion of settlements and infrastructure accounted for a relatively small percent of tree cover loss globally (1.5±0.5%, 2.2±0.7%, and 1.2±0.3%, respectively), but were important regional drivers. For example, in Southeast Asia and Asia, a relatively higher proportion of loss was attributed to the establishment and expansion of hard commodities— 2.4±1.5% and 1.7±0.7% of loss, respectively. Other natural disturbances represented 3.9±2.2% in North America and 3.5±2.1% of loss in Asia. Disease and insect outbreaks, such as bark beetle, were common in Asia and North America and caused large-scale loss in those regions. Expansion of settlements and infrastructure represented 2.4±1.2% of loss in North America and 2.4±1.8% in Europe, primarily around urban centers (Figure 4).
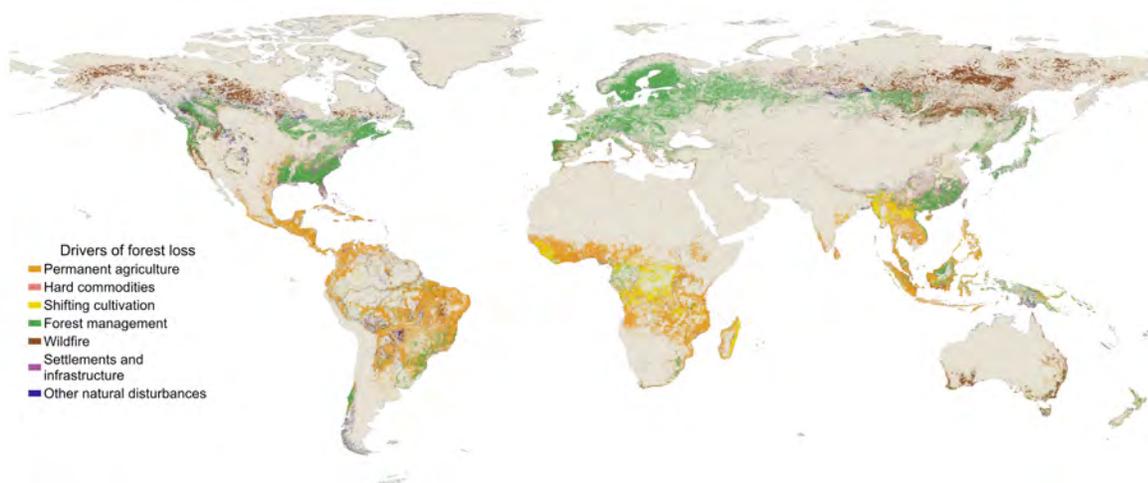
Figure 3. Global drivers of forest loss.

Figure 4. Examples of global drivers of forest loss at 1 km resolution. Color opacity corresponds to tree cover loss intensity within each 1 km grid cell. The Global Forest Change tree cover loss data at 30 m resolution is displayed in white beneath the drivers of forest loss map. a) Gold mining, natural river meandering, and agriculture expansion in Madre de Dios, Peru (lon: -70.5378, lat: -12.7778), and b) Planet imagery from 2022. c) Palm oil plantations surrounding by selective logging in Sarawak, Malaysia (lon: 114.1137, lat: 3.2739) and d) Planet imagery from 2019 (following selective logging in 2017 and 2018). e) Shifting cultivation in the Democratic Republic of Congo (lon: 19.0567, lat: 0.5707), and f) Planet imagery from 2022. g) Urban expansion in North Carolina, United States (lon: -78.8480, lat: 35.7784) and h) Sentinel-2 imagery from 2021.

Table 3. Global and regional map-based and sample-based attribution of the proportion of total tree cover loss by driver. Map-based estimates were calculated using the Global Forest Change tree cover loss data from 2001-2022 overlaid with our drivers of forest loss map. Sample-based estimates are based on the validation sample and derived using a ratio estimator. Sample-based values include ±95% confidence interval. *Indicates drivers associated with permanent deforestation.

Region	Perm ag*	Hard com*	Shifting cult	Forest man	Wildfire	Settle & infra*	Other nat dist
North America							
Map	2.7%	0.6%	0.0%	48.2%	45.0%	1.9%	1.7%
Sample	3.0±2.7%	1.1±1.3%	0.0±0.0%	44.7±6.1%	44.9±5.7%	2.4±1.2%	3.9±2.2%
Latin America							
Map	73.8%	0.7%	3.2%	11.5%	8.2%	0.4%	2.1%
Sample	68.7±5.7%	1.5±1.6%	4.0±1.7%	11.0±4.4%	13.4±3.9%	0.3±0.2%	1.1±0.5%
Europe							
Map	1.6%	0.4%	0.0%	88.9%	7.6%	1.3%	0.2%
Sample	3.8±2.4%	0.4±0.3%	0.0±0.0%	85.5±4.4%	7.3±3.3%	2.4±1.8%	0.6±0.5%
Africa							
Map	53.0%	0.5%	38.9%	4.3%	1.8%	1.0%	0.5%
Sample	51.1±6.6%	1.2±0.9%	36.6±6.5%	3.2±2.3%	5.6±2.1%	1.1±0.8%	1.1±0.6%
Asia							
Map	2.5%	1.0%	1.5%	26.3%	65.4%	1.4%	1.9%
Sample	3.9±1.9%	1.7±0.7%	1.3±0.6%	23.0±5.1%	65.5±5.3%	1.0±0.5%	3.5±2.1%
Southeast Asia							
Map	65.7%	1.8%	14.8%	12.6%	3.7%	0.8%	0.7%
Sample	61.3±6.7%	2.4±1.5%	11.1±4.0%	18.2±5.4%	3.9±2.1%	1.2±0.9%	1.9±1.5%
Oceania							
Map	6.0%	0.7%	4.3%	20.3%	66.5%	0.7%	1.5%
Sample	11.2±4.4%	0.8±1.0%	4.4±1.4%	15.5±4.1%	66.1±5.4%	0.6±0.3%	1.4±0.5%
Global							
Map	34.4%	0.8%	8.5%	25.2%	28.5%	1.1%	1.5%
Sample	34.8±2.6%	1.5±0.5%	7.9±1.3%	23.1±2.2%	29.3±2.3%	1.2±0.3%	2.2±0.7%

3.2. Drivers of permanent and temporary forest loss

Permanent agriculture, hard commodities, and expansion of settlements and infrastructure are likely to represent a permanent land use change from forest to non-forest and are therefore indicative of deforestation. Globally, 37% of permanent tree cover loss was attributed to these drivers, primarily due to permanent agriculture (Table 3). Wildfire, forest management, shifting cultivation, and other natural disturbances are more likely to represent temporary disturbances that may be followed by forest regrowth. These drivers were associated with 63% of loss globally, of which 47% were associated with wildfire and 37% were associated with forest management. Although these disturbances are often temporary, they may lead to degradation, such as logging in primary forests, intensification of shifting cultivation, or wildfires in non-fire adapted ecosystems, such as humid tropical forests [7, 5, 58].

Drivers likely to represent deforestation were associated with the majority of loss in Latin America (71%) and Southeast Asia (65%), and just over half of loss in Africa

(53%). Drivers representing temporary disturbances were associated with the majority of loss in North America (93%), Europe (93%), Asia (93%), and Oceania (87%).

3.3. Accuracy assessment

To assess the quality of our map, we performed an accuracy assessment of the map results against the validation data. The driver attribution model's global overall accuracy was 90.5±1.4% (Table 4). Global per class producer's and user's accuracy were highest for the permanent agriculture, forest management, and wildfire classes (over 90% for both user's and producer's accuracy) (Figure 5). Global user's and producer's accuracy was lower for rarer classes, such as settlements and infrastructure and other natural disturbances. The map-based estimates largely fall within the confidence intervals of the sample-based estimates (Table 3), suggesting that in future applications the map can be used to directly quantify the the drivers of forest loss.

All regions except Southeast Asia and Africa had an overall accuracy of 90% or higher (Table 4). Regional user's and producer's accuracies per class were generally high (frequently over 80% for user's accuracy and 70% for producer's accuracy) but varied by region (Figure 5). Higher accuracy was obtained for the driver class that was predominant in each region and for forest management across all regions. Other natural disturbances and hard commodities, on the other hand, had lower producer's accuracy and higher standard error due to their heterogeneous characteristics (Table S5). In Europe, rarer classes such as permanent agriculture and hard commodities had lower accuracy relative to rare classes in other regions. This is likely due to the fact that forest loss related to these drivers is very small-scale in Europe and harder to detect and correctly classify at 1 km resolution.

Table 4. Overall accuracy and ±95% confidence interval by region

Region	Overall accuracy
North America	92.4±3.7
Europe	93.8±3.1
Africa	87.4±4.2
Asia	94.1±2.4
Southeast Asia	82.8±5.1
Oceania	90.2±3.9
Latin America	90.7±3.0
Global	90.5±1.4

3.4. Comparison with prior estimates

Compared with Curtis *et al.* [13], our approach enabled the improved differentiation of drivers that may have similar spatial patterns, such as small scale commodity crop
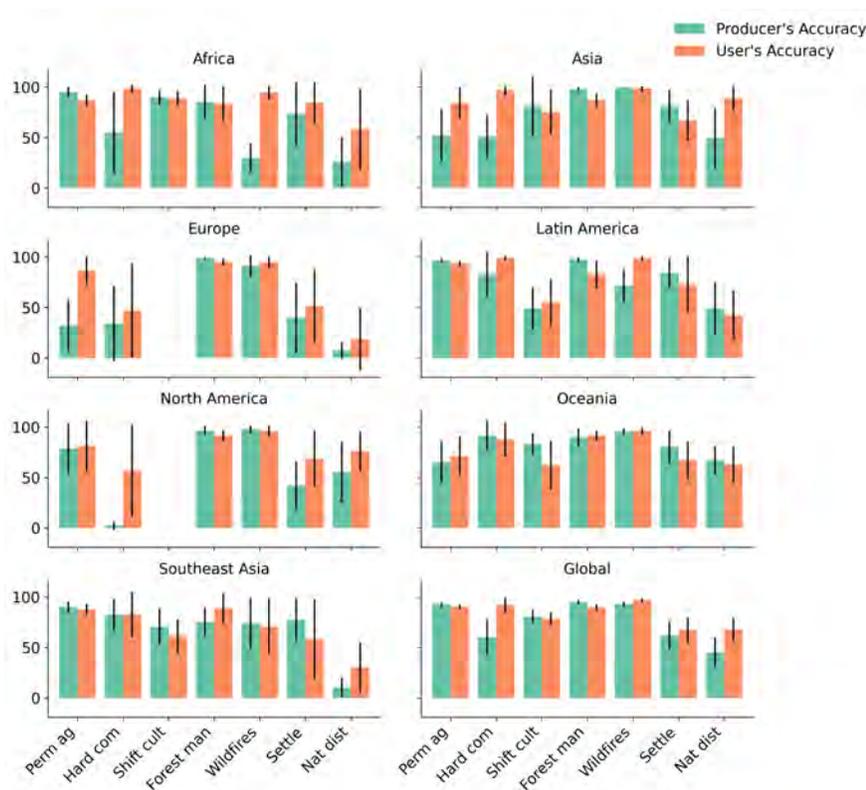
Figure 5. User's and producer's accuracy per region with 95% confidence interval. The *shifting cultivation* class does not occur in Europe or North America.

production and shifting cultivation. The higher spatial resolution and thematic detail of our map also allowed for better detection of small-scale drivers, such as small wildfires, settlements and infrastructure, and selective logging (Figure 6).

Globally, our map attributed 15% more loss to permanent agriculture and hard commodities (Table 5). This is mostly due to the smaller proportion of loss attributed to shifting cultivation in our map (16% less than Curtis *et al.*) as a result of better differentiating it from permanent agriculture. The difference between these classes varied by region. In Southeast Asia, our map attributed 12% more loss to shifting cultivation. In Africa, on the other hand, Curtis *et al.* attributed only 1% of loss to commodity-driven deforestation and 95% to shifting cultivation, while our map attributed 54% and 39%, respectively. This was likely due to the predominance of small-scale agriculture in this region. Curtis *et al.* included many types of small-scale agriculture in their shifting cultivation class [13], while our map separated permanent agricultural systems — which can include small-scale and subsistence agriculture — from shifting cultivation.

Forestry and wildfire were widespread drivers according to both maps, although their relative importance was different — wildfire represented a larger area in our map (29% relative to 23% in Curtis *et al.*), while forest management represented a smaller area (25% relative to 31%). A higher proportion of loss was attributed to wildfire in our

map across all regions.
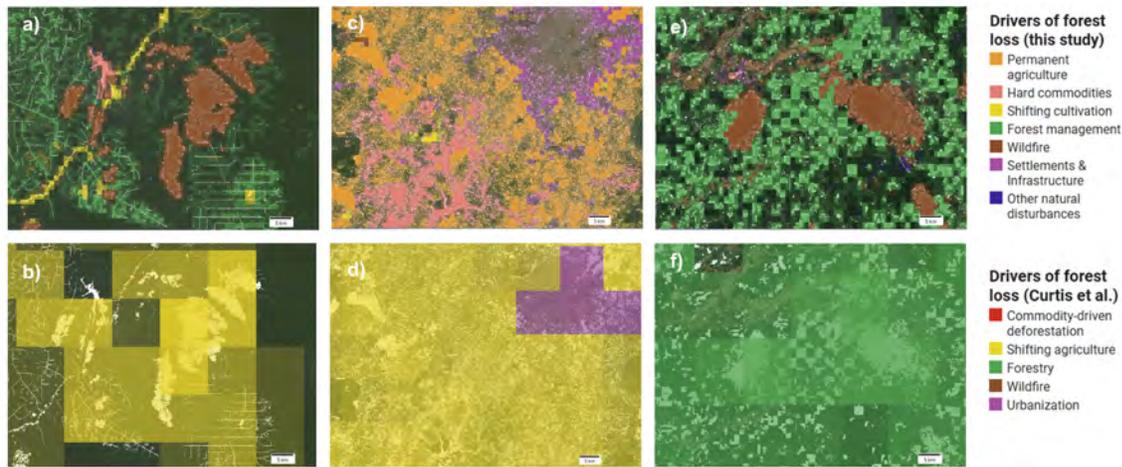
Figure 6. Comparison of the drivers of forest loss map at 1 km produced from this study with the drivers of forest loss map at 10 km from Curtis *et al.* [13] (updated to 2022). Color opacity corresponds to tree cover loss intensity within each grid cell. The Global Forest Change tree cover loss data at 30 m resolution is displayed in white beneath the drivers of forest loss maps. a) Our map of the drivers of forest loss at 1 km detects selective logging, fires, and flooding for hydropower in Congo (lon: 15.8601, lat: 1.0377). b) The Curtis et al. map in the same location classifies all loss as shifting agriculture. c) Our map detects mining, smallholder cocoa production, and urban expansion outside Kumasi, Ghana (lon: -1.7699, lat: 6.5257). d) The Curtis et al. map in the same location classifies shifting agriculture and urban expansion. e) Our map differentiates small scale fires from logging in Oregon, USA (lon:-123.1427, lat:42.8824). f) The Curtis et al. map in the same location classifies all loss as forestry.

4. Discussion

Our study presents a globally consistent wall-to-wall map of the drivers of forest loss. The higher spatial and thematic resolution relative to prior global studies [13] allows for a better characterization of forest disturbance dynamics in regions where multiple drivers are co-located, as well as a more nuanced distinction of drivers that result in permanent forest loss (deforestation) versus temporary disturbances.

4.1. Permanent agriculture and shifting cultivation

Both permanent agriculture and shifting cultivation play a substantial role in driving tree cover loss globally, particularly in tropical regions. Although previous studies show similar findings [13, 59, 46], our study represents an advancement in separating permanent from

Table 5. Comparison of estimates of the proportion of total tree cover loss attributed to each driver from this study and Curtis *et al.* (updated to 2022). Estimates were calculated using the Global Forest Change tree cover loss data from 2001-2022 overlaid with each drivers of forest loss map. For this comparison, the *permanent agriculture* and *hard commodities* classes from our map were grouped together and compared with the *commodity-driven deforestation* class from Curtis *et al.*

Region	Perm ag & hard com	Shifting cult	Forest man	Wildfire	Settle & infra
North America					
This study	3.2%	0.0%	48.2%	45.0%	1.9%
Curtis *et al.*	1.1%	0.3%	59.1%	36.2%	3.3%
Latin America					
This study	74.5%	3.2%	11.5%	8.2%	0.4%
Curtis *et al.*	41.0%	42.8%	15.5%	0.5%	0.1%
Europe					
This study	2.0%	0.0%	88.9%	7.6%	1.3%
Curtis *et al.*	0.0%	1.0%	98.5%	0.4%	0.1%
Africa					
This study	53.6%	38.9%	4.3%	1.8%	1.0%
Curtis *et al.*	1.0%	94.9%	3.0%	0.5%	0.6%
Asia					
This study	3.6%	1.5%	26.3%	65.4%	1.4%
Curtis *et al.*	0.4%	0.8%	39.6%	59.2%	0.0%
Southeast Asia					
This study	67.5%	14.8%	12.6%	3.7%	0.8%
Curtis *et al.*	87.3%	3.3%	9.2%	0.0%	0.2%
Oceania					
This study	6.6%	4.3%	20.3%	66.5%	0.7%
Curtis *et al.*	0.8%	12.2%	22.5%	62.9%	1.6%
Global					
This study	35.2%	8.5%	25.2%	28.5%	1.1%
Curtis *et al.*	20.6%	24.8%	31.2%	22.5%	0.8%

cyclical cultivation and shows that a large proportion of what was previously mapped as temporary loss in the form of shifting cultivation may actually represent deforestation in the form of permanent agriculture. Shifting cultivation, a form of subsistence farming, has existed in the tropics for millennia [63], but is increasingly being replaced by commodity crops [30, 81]. A better understanding of this nuance in land use dynamics is critical as temporary disturbances and deforestation have markedly different implications for both carbon cycling and biodiversity. While forests under shifting cultivation typically undergo periods of recovery, allowing for carbon sequestration, habitat regeneration, and recuperation of soil fertility, permanent conversion to agriculture represents a long-term carbon stock loss and more profound habitat disruption [39]. Note, however, that population growth has led to intensification of shifting cultivation systems in recent decades, making the environmental impacts of this practice highly dependent on context [81, 87].

Furthermore, permanent agriculture is often the focus of companies that aim to eliminate commodity crop-driven deforestation from their supply chains. Therefore,

making the distinction between permanent agriculture and shifting cultivation is critical for devising appropriate management interventions and land use policies. Our results suggest that policies requiring full traceability for deforestation risk commodities are necessary to abate the continued expansion of agriculture at the expense of forests. However, it is critical to note that our attribution of tree cover loss to permanent agriculture includes both trade-oriented commodity crop production and permanent small-scale agriculture for subsistence, which represent different underlying dynamics and require distinct policy responses. Consideration of local context should guide strategies for equitable outcomes [69].

4.2. Other natural disturbances and wildfires

Our study is a major advancement in mapping other natural disturbances globally, detecting events such as bark beetle outbreaks in the Western United States, Canada, and Russia; hurricane damage in the Caribbean; landslides; as well as natural cycles of forest loss caused by river meandering and windthrow, for example (Figure 7). Although these disturbances can play an important role in maintaining forest ecosystem health, climate change has exacerbated the extent, frequency, or severity of many natural disturbance events, in some cases increasing the risk of subsequent disturbances and eventual forest degradation. For example, the warming and drying effects of climate change have led to dramatic increases in bark beetle outbreaks in some regions [19, 37], which can increase the severity of impacts from subsequent disturbances, such as wildfire [83]. Our study also highlights the dominance of wildfire as a driver of forest loss, in line with findings from other studies [80]. Similarly, although wildfires play an important role in fire-adapted temperate and boreal forests, increasing fire frequency and severity — driven in part by climate change — can impede their ability to recover [10]. In non-fire adapted ecosystems, such as the humid tropics, fires can lead to forest degradation [7].

4.3. Regional importance of mining and energy infrastructure

Although a relatively minor driver globally, our study is an advancement in mapping hard commodities, which have outsized impacts at local and regional scales. Attribution of forest loss to hard commodities is critical since the establishment of these activities often leads to long-lasting, acute and localized environmental impacts [65, 88, 17]. Our map identified diverse regional dynamics, such as oil drilling in boreal regions of Canada and Russia, widespread hydroelectric dam creation in Southeast Asia, and expansion of mining across multiple regions (Figure 8). Mining, in particular, can have severe impacts on local ecosystems and human health, including pollution and exposure to toxins [18], negative impacts on water quality and availability [17], and ecosystem degradation and biodiversity loss [3, 88].
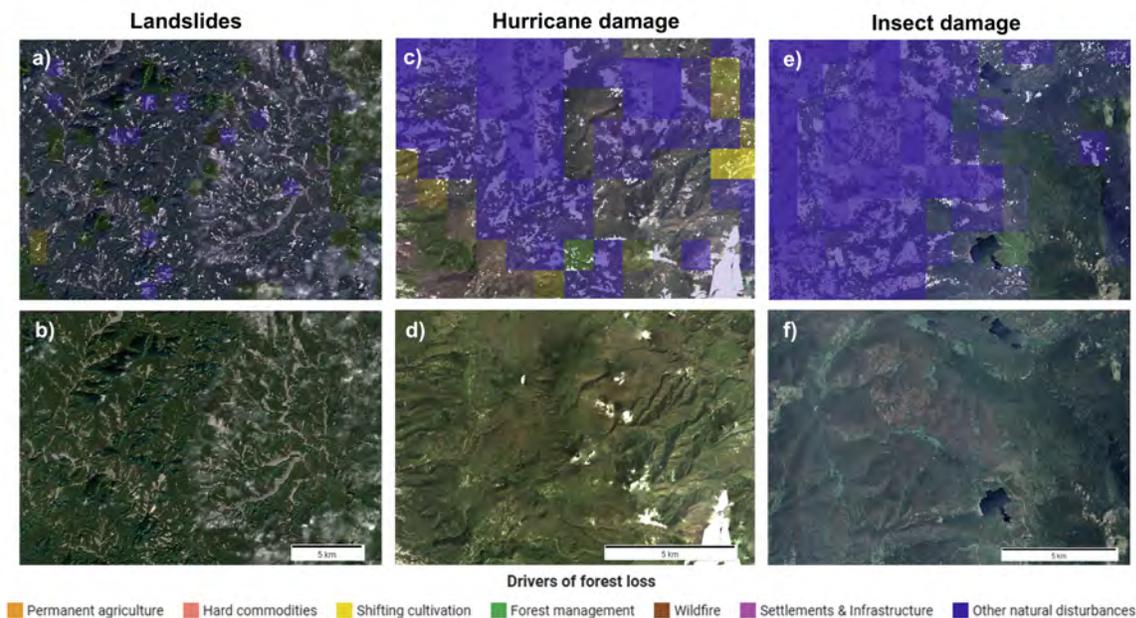
Figure 7. Examples from the *other natural disturbances* driver of forest loss class at 1 km resolution. Color opacity corresponds to tree cover loss intensity within each 1 km grid cell. The Global Forest Change tree cover loss data at 30 m resolution is displayed in white beneath the drivers of forest loss map. a) Landslides following Typhoon Morakot in 2009 in southern Taiwan (lon: 120.8157, lat: 22.9844) and b) Sentinel-2 composites from 2021, with landslide debris still visible. c) Damage from Hurricane Maria in 2017 in Dominica (lon: -61.3357, lat: 15.3757) and d) Planet imagery from 2017 showing tree mortality. e) Mountain pine beetle outbreak in the early 2000s in Arapaho National Forest, Colorado, USA (lon: -105.7764, lat: 40.0843) and f) NAIP imagery from 2009 showing tree mortality.

4.4. Limitations

There are several important limitations to this work. First, our model and resulting maps are limited in scope to classifying the driver of forest loss as mapped by the GFC product [26], and therefore the detection and quantification of loss is subject to the accuracy of that product. Second, tree cover loss as defined by [26] includes disturbances in both natural and planted forests. In this study, we do not distinguish between the loss of natural forest and planted forest (e.g., plantations, agroforestry systems, or other planted trees). While we consider tree cover loss associated with the permanent agriculture, hard commodities, and settlements and infrastructure classes to represent a close approximation of deforestation (section S4), users should note that these classes do not always represent the conversion of *natural* forests to other land uses. Similarly, replacement of natural forest with wood fiber plantations is not distinguished from routine harvesting within existing plantations established before 2000, as these are both included in the forest management class. Third, our study includes salvage and sanitation
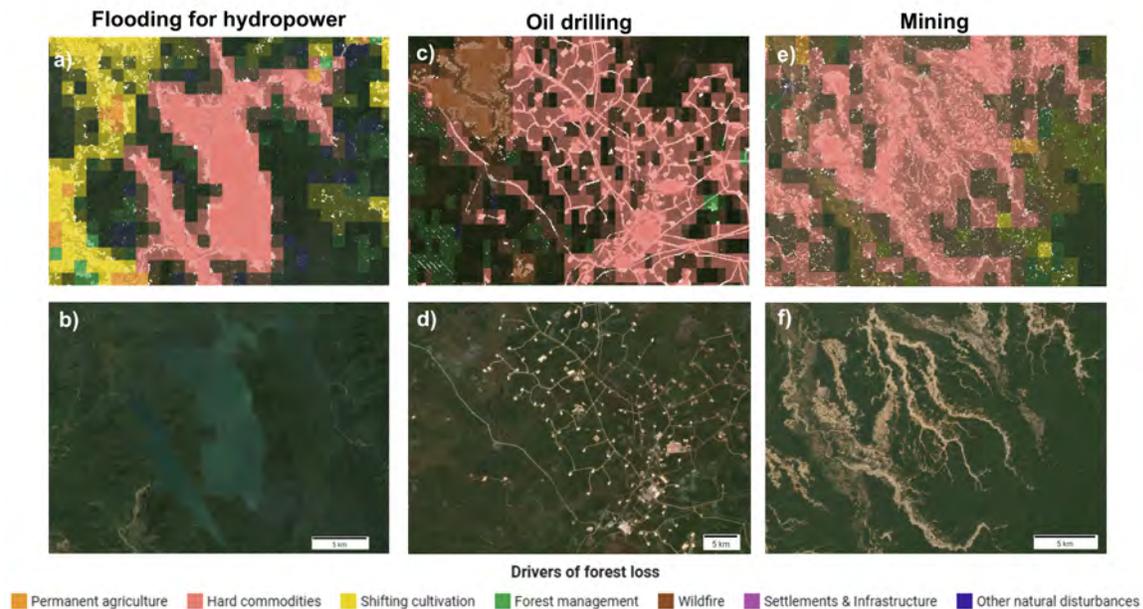
Figure 8. Examples from the *hard commodities* driver of forest loss class at 1 km resolution. Color opacity corresponds to tree cover loss intensity within each 1 km grid cell. The Global Forest Change tree cover loss data at 30 m resolution is displayed in white beneath the drivers of forest loss map. a) Flooding for the construction of the Xekaman 1 hydropower plant in Laos (lon: 107.2103, lat: 15.01915) and b) Planet composite from 2022. c) Oil drilling in the Lensky District, Russia (lon: 110.8553, lat: 59.8539) and d) Sentinel-2 composite from 2020. e) Gold mining in Myanmar (lon: 95.0379, lat: 24.598) and f) Planet composite from 2022.

logging in the forest management class, due to the challenges of disentangling natural disturbances from salvage logging when they occur in quick succession. Finally, because we map the dominant driver of tree cover loss within each 1 km grid from 2001-2022, we do not disentangle different drivers that are co-located at scales smaller than 1 km. In some highly heterogeneous landscapes with mosaics of various land uses, multiple drivers of forest loss can occur in close proximity. Future work should prioritize mapping drivers of forest loss at a higher temporal resolution (e.g., annually) and spatial resolution (e.g., 30 m pixel scale or disturbance scale) in order to understand the temporal sequence of drivers at small spatial scales.

5. Conclusion

This study presents the first global map of the drivers of forest loss at 1 km resolution for 2001-2022, substantially improving the spatial and thematic detail of existing global maps [13]. This model is trained on satellite data from various sensors and ancillary biophysical and population data, many of which are updated at an annual or sub-annual cadence, allowing for our model to be updated regularly to support forest monitoring

efforts. A better characterization of the direct drivers of forest loss can support the development of forest conservation and management policies, alert relevant industry and government bodies to the risks of carbon emissions and biodiversity loss within their supply chains and jurisdictions, and track progress towards global goals to end deforestation. We intend to update the drivers of forest loss map alongside annual updates to the GFC product [26].

6. Acknowledgments

7. Data availability statement

The global map of drivers of forest loss at 1 km and the associated class probabilities, as well as the training and validation samples, will be available upon publication.

8. Author contribution statement

Michelle Sims: Conceptualization, Data curation, Formal analysis, Methodology, Software, Validation, Project administration, Visualization, Writing- original draft, Writing- review & editing.
Radost Stanimirova: Conceptualization, Data curation, Formal analysis, Methodology, Software, Validation, Project administration, Visualization, Writing- original draft, Writing- review & editing.
Anton Raichuk: Formal analysis, Investigation, Methodology, Software, Validation, Resources.
Maxim Neumann: Supervision, Formal analysis, Investigation, Methodology, Software, Project administration, Validation, Resources, Visualization, Writing- original draft, Writing- review & editing.
Jessica Richter: Data curation, Validation, Writing- review & editing.
Forrest Follett: Conceptualization, Formal analysis, Writing- original draft, Writing- review & editing.
James MacCarthy: Conceptualization, Software, Writing- review & editing.
Kristine Lister: Conceptualization, Data curation, Writing- review & editing.
Christopher Randle: Data curation, Writing- review & editing.
Lindsey Sloat: Conceptualization, Supervision, Writing- review & editing.

Charlotte Stanton: Resources, Writing- review & editing.

Dan Morris: Resources, Writing- review & editing.

Elena Esipova: Data curation, Validation.

Jaelah Jupiter: Data curation, Validation.

Christy Melhart Slay: Conceptualization, Supervision, Writing- review & editing.

Drew Purves: Supervision, Resources, Writing- review & editing.

Nancy Harris: Conceptualization, Funding Acquisition, Supervision, Writing- review & editing.

References

[1] Digital Earth Africa. Cropland extent maps for africa, 2022.

[2] Anurag Arnab, Mostafa Dehghani, Georg Heigold, Chen Sun, Mario Lučić, and Cordelia Schmid. Vivit: A video vision transformer. In *International Conference on Computer Vision (ICCV)*, 2021.

[3] Bora Aska, Daniel M. Franks, Martin Stringer, and Laura J. Sonter. Biodiversity conservation threatened by global mining wastes. *Nature Sustainability*, 7(1):23–30, January 2024.

[4] Kemen G. Austin, Amanda Schwantes, Yaofeng Gu, and Prasad S. Kasibhatla. What causes deforestation in Indonesia? *Environmental Research Letters*, 14(2):024007, February 2019. Publisher: IOP Publishing.

[5] Jos Barlow, Gareth D. Lennox, Joice Ferreira, Erika Berenguer, Alexander C. Lees, Ralph Mac Nally, James R. Thomson, Silvio Frosini de Barros Ferraz, Julio Louzada, Victor Hugo Fonseca Oliveira, Luke Parry, Ricardo Ribeiro de Castro Solar, Ima C. G. Vieira, Luiz E. O. C. Aragão, Rodrigo Anzolin Begotti, Rodrigo F. Braga, Thiago Moreira Cardoso, Raimundo Cosme de Oliveira, Carlos M. Souza Jr, Nárgila G. Moura, Sâmia Serra Nunes, João Victor Siqueira, Renata Pardini, Juliana M. Silveira, Fernando Z. Vaz-de Mello, Ruan Carlo Stulpen Veiga, Adriano Venturieri, and Toby A. Gardner. Anthropogenic disturbance in tropical forests can double biodiversity loss from deforestation. *Nature*, 535(7610):144–147, July 2016. Publisher: Nature Publishing Group.

[6] Matthew G. Betts, Zhiqiang Yang, Adam S. Hadley, Adam C. Smith, Josée S. Rousseau, Joseph M. Northrup, Joseph J. Nocera, Noel Gorelick, and Brian D. Gerber. Forest degradation drives widespread avian habitat and population declines. *Nature Ecology & Evolution*, 6(6):709–719, June 2022. Publisher: Nature Publishing Group.

[7] C. Bourgoin, G. Ceccherini, M. Girardello, C. Vancutsem, V. Avitabile, P. S. A. Beck, R. Beuchle, L. Blanc, G. Duveiller, M. Migliavacca, G. Vieilledent, A. Cescatti, and F. Achard. Human degradation of tropical moist forests is greater than previously estimated. *Nature*, 631(8021):570–576, July 2024.

[8] Leo Breiman. Bagging predictors. *Machine learning*, 24(2):123–140, 1996.

[9] Christopher F. Brown, Steven P. Brumby, Brookie Guzder-Williams, Tanya Birch, Samantha Brooks Hyde, Joseph Mazzariello, Wanda Czerwinski, Valerie J. Pasquarella, Robert Haertel, Simon Ilyushchenko, Kurt Schwehr, Mikaela Weisse, Fred Stolle, Craig Hanson, Oliver Guinan, Rebecca Moore, and Alexander M. Tait. Dynamic world, near real-time global 10 m land use land cover mapping. *Scientific Data*, 9(1):251, June 2022.

[10] Arden Burrell, Elena Kukavskaya, Robert Baxter, Qiaoqi Sun, and Kirsten Barrett. *Post-fire Recruitment Failure as a Driver of Forest to Non-forest Ecosystem Shifts in Boreal Regions*, page 69–100. Springer International Publishing, Cham, 2021.

[11] Shijuan Chen, Pontus Olofsson, Thatheva Saphangthong, and Curtis E. Woodcock. Monitoring shifting cultivation in Laos with Landsat time series. *Remote Sensing of Environment*, 288:113507, April 2023.

[12] Nicola Clerici, Christina Staudhammer, and Francisco J. Escobedo. Disentangling the deforestation-environmental crime nexus in latin america. *Trees, Forests and People*, 17:100610, September 2024.

[13] Philip G. Curtis, Christy M. Slay, Nancy L. Harris, Alexandra Tyukavina, and Matthew C. Hansen. Classifying drivers of global forest loss. *Science*, 361(6407):1108–1111, September 2018.

[14] Teresa De Marzo, Nestor Ignacio Gasparri, Eric F. Lambin, and Tobias Kuemmerle. Agents of Forest Disturbance in the Argentine Dry Chaco. *Remote Sensing*, 14(7):1758, January 2022. Number: 7 Publisher: Multidisciplinary Digital Publishing Institute.

[15] V De Sy, M Herold, F Achard, V Avitabile, A Baccini, S Carter, J G P W Clevers, E Lindquist, Maria Pereira, and L Verchot. Tropical deforestation drivers and associated carbon emission factors derived from remote sensing data. *Environmental Research Letters*, 14(9):094022, September 2019.

[16] V. De Sy, M. Herold, F. Achard, R. Beuchle, J. G. P. W. Clevers, E. Lindquist, and L. Verchot. Land use patterns and related carbon losses following deforestation in South America. *Environmental Research Letters*, 10(12):124004, November 2015. Publisher: IOP Publishing.

[17] Evan N. Dethier, Miles Silman, Jimena Díaz Leiva, Sarra Alqahtani, Luis E. Fernandez, Paúl Pauca, Seda Çamalan, Peter Tomhave, Francis J. Magilligan, Carl E. Renshaw, and David A. Lutz. A global rise in alluvial mining increases sediment load in tropical rivers. *Nature*, 620(7975):787–793, August 2023.

[18] Sarah E. Diringer, Beth J. Feingold, Ernesto J. Ortiz, John A. Gallis, Julio M. Araújo-Flores, Axel Berky, William K. Y. Pan, and Heileen Hsu-Kim. River transport of mercury from artisanal and small-scale gold mining and risks for dietary mercury exposure in madre de dios, peru. *Environmental Science: Processes & Impacts*, 17(2):478–487, February 2015.

[19] Christopher J Fettig, Christopher Asaro, John T Nowak, Kevin J Dodds, Kamal J K Gandhi, Jason E Moan, and Jeanne Robert. Trends in bark beetle impacts in north america during a period (2000–2020) of rapid environmental change. *Journal of Forestry*, 120(6):693–713, November 2022.

[20] Matt Finer, Sidney Novoa, Mikaela J. Weisse, Rachael Petersen, Joseph Mascaro, Tamia Souto, Forest Stearns, and Raúl García Martinez. Combating deforestation: From satellite to intervention. *Science*, 360(6395):1303–1305, June 2018.

[21] Maegan Fitzgerald, Janet Nackoney, Peter Potapov, and Svetlana Turubanova. Agriculture is the primary driver of tree cover loss across the Forestière region of the Republic of Guinea, Africa. *Environmental Research Communications*, 3(12):121004, December 2021. Publisher: IOP Publishing.

[22] Jonathan A. Foley, Ruth DeFries, Gregory P. Asner, Carol Barford, Gordon Bonan, Stephen R. Carpenter, F. Stuart Chapin, Michael T. Coe, Gretchen C. Daily, Holly K. Gibbs, Joseph H. Helkowski, Tracey Holloway, Erica A. Howard, Christopher J. Kucharik, Chad Monfreda, Jonathan A. Patz, I. Colin Prentice, Navin Ramankutty, and Peter K. Snyder. Global Consequences of Land Use. *Science*, 309(5734):570–574, July 2005. Publisher: American Association for the Advancement of Science.

[23] Yan Gao, Margaret Skutsch, Jaime Paneque-Gálvez, and Adrian Ghilardi. Remote sensing of forest degradation: a review. *Environmental Research Letters*, 15(10):103001, September 2020. Publisher: IOP Publishing.

[24] L. Giglio, Christopher Justice, L. Boschetti, and David Roy. MODIS/Terra+Aqua Burned Area Monthly L3 Global 500m SIN Grid V061, 2021.

[25] Noel Gorelick, Matt Hancher, Mike Dixon, Simon Ilyushchenko, David Thau, and Rebecca Moore. Google Earth Engine: Planetary-scale geospatial analysis for everyone. *Remote Sensing of Environment*, 202:18–27, December 2017.

[26] M. C. Hansen, P. V. Potapov, R. Moore, M. Hancher, S. A. Turubanova, A. Tyukavina, D. Thau, S. V. Stehman, S. J. Goetz, T. R. Loveland, A. Kommareddy, A. Egorov, L. Chini, C. O. Justice, and J. R. G. Townshend. High-Resolution Global Maps of 21st-Century Forest Cover Change. *Science*, 342(6160):850–853, November 2013.

[27] Nancy L. Harris, David A. Gibbs, Alessandro Baccini, Richard A. Birdsey, Sytze De Bruin, Mary Farina, Lola Fatoyinbo, Matthew C. Hansen, Martin Herold, Richard A. Houghton, Peter V. Potapov, Daniela Requena Suarez, Rosa M. Roman-Cuesta, Sassan S. Saatchi, Christy M. Slay, Svetlana A. Turubanova, and Alexandra Tyukavina. Global maps of twenty-first century forest carbon fluxes. *Nature Climate Change*, 11(3):234–240, March 2021.

[28] Laurence Hawker, Peter Uhe, Luntadila Paulo, Jeison Sosa, James Savage, Christopher Sampson, and Jeffrey Neal. A 30 m global map of elevation with forests and buildings removed. *Environmental Research Letters*, 17(2):024016, February 2022.

[29] Kaiming He, X. Zhang, Shaoqing Ren, and Jian Sun. Deep residual learning for image recognition. *2016 IEEE Conference on Computer Vision and Pattern Recognition (CVPR)*, pages 770–778, 2015.

[30] Andreas Heinimann, Ole Mertz, Steve Frolking, Andreas Egelund Christensen, Kaspar Hurni, Fernando Sedano, Louise Parsons Chini, Ritvik Sahajpal, Matthew Hansen, and George Hurtt. A global view of shifting cultivation: Recent, current, and future extent. *PLOS ONE*, 12(9):e0184479, September 2017.

[31] Sabine Henders, Madelene Ostwald, Vilhelm Verendel, and Pierre Ibisch. Do national strategies under the UN biodiversity and climate conventions address agricultural commodity consumption as deforestation driver? *Land Use Policy*, 70:580–590, January 2018.

[32] Txomin Hermosilla, Michael A. Wulder, Joanne C. White, and Nicholas C. Coops. Prevalence of multiple forest disturbances and impact on vegetation regrowth from interannual Landsat time series (1985–2015). *Remote Sensing of Environment*, 233:111403, November 2019.

[33] Paul F. Hessburg, Susan J. Prichard, R. Keala Hagmann, Nicholas A. Povak, and Frank K. Lake. Wildfire and climate change adaptation of western North American forests: a case for intentional management. *Ecological Applications*, 31(8):e02432, 2021. _eprint: https://onlinelibrary.wiley.com/doi/pdf/10.1002/eap.2432.

[34] M. G. Hethcoat, D. P. Edwards, J. M. B. Carreiras, R. G. Bryant, F. M. França, and S. Quegan. A machine learning approach to map tropical selective logging. *Remote Sensing of Environment*, 221:569–582, February 2019.

[35] Noriko Hosonuma, Martin Herold, Veronique De Sy, Ruth S. De Fries, Maria Brockhaus, Louis Verchot, Arild Angelsen, and Erika Romijn. An assessment of deforestation and forest degradation drivers in developing countries. *Environmental Research Letters*, 7(4):044009, October 2012. Publisher: IOP Publishing.

[36] Lian-Zhi Huo, Luigi Boschetti, and Aaron M. Sparks. Object-Based Classification of Forest Disturbance Types in the Conterminous United States. *Remote Sensing*, 11(5):477, January 2019. Number: 5 Publisher: Multidisciplinary Digital Publishing Institute.

[37] Luciana Jaime, Enric Batllori, and Francisco Lloret. Bark beetle outbreaks in coniferous forests: a review of climate change effects. *European Journal of Forest Research*, 143(1):1–17, February 2024.

[38] Nikolai Kalischek, Nico Lang, Cécile Renier, Rodrigo Caye Daudt, Thomas Addoah, William Thompson, Wilma J. Blaser-Hart, Rachael Garrett, Konrad Schindler, and Jan D. Wegner. Cocoa plantations are associated with deforestation in Côte d'Ivoire and Ghana. *Nature Food*, 4(5):384–393, May 2023.

[39] Teegalapalli Karthik, Gopi Govindhan Veeraswami, and Prasanna Kumar Samal. Forest recovery following shifting cultivation: An overview of existing research. *Tropical Conservation Science*, December 2009.

[40] Robert E. Kennedy, Zhiqiang Yang, Justin Braaten, Catharine Copass, Natalya Antonova, Chris Jordan, and Peder Nelson. Attribution of disturbance change agent from Landsat time-series in support of habitat monitoring in the Puget Sound region, USA. *Remote Sensing of Environment*, 166:271–285, September 2015.

[41] Diederik P. Kingma and Jimmy Ba. Adam: A method for stochastic optimization, 2014.

[42] Alexander Kolesnikov, Lucas Beyer, Xiaohua Zhai, Joan Puigcerver, Jessica Yung, Sylvain Gelly, and Neil Houlsby. Big transfer (bit): General visual representation learning. In *Computer Vision – ECCV 2020*, page 491–507. Springer International Publishing, 2020.

[43] Alexander Kolesnikov, Alexey Dosovitskiy, Dirk Weissenborn, Georg Heigold, Jakob Uszkoreit, Lucas Beyer, Matthias Minderer, Mostafa Dehghani, Neil Houlsby, Sylvain Gelly, Thomas Unterthiner, and Xiaohua Zhai. An image is worth 16x16 words: Transformers for image recognition at scale. In *International Conference on Learning Representations (ICLR)*, 2021.

[44] Moritz Kramer, Tobias Kind-Rieper, Raquel Munayer, Stefan Giljum, Rens Masselink, Pia van Ackern, Victor Maus, Sebastian Luckender, Nikolas Kuschnig, Felipe Costa, and Lukas Ruttinger. *Extracted Forests*. Berlin, 2023.

[45] David M. Lapola, Patricia Pinho, Jos Barlow, Luiz E. O. C. Aragão, Erika Berenguer, Rachel Carmenta, Hannah M. Liddy, Hugo Seixas, Camila V. J. Silva, Celso H. L. Silva-Junior, Ane A. C. Alencar, Liana O. Anderson, Dolors Armenteras, Victor Brovkin, Kim Calders, Jeffrey Chambers, Louise Chini, Marcos H. Costa, Bruno L. Faria, Philip M. Fearnside, Joice Ferreira, Luciana Gatti, Victor Hugo Gutierrez-Velez, Zhangang Han, Kathleen Hibbard, Charles Koven, Peter Lawrence, Julia Pongratz, Bruno T. T. Portela, Mark Rounsevell, Alex C. Ruane, Rüdiger Schaldach, Sonaira S. Da Silva, Celso Von Randow, and Wayne S. Walker. The drivers and impacts of Amazon forest degradation. *Science*, 379(6630):eabp8622, January 2023.

[46] Juan Carlos Laso Bayas, Linda See, Ivelina Georgieva, Dmitry Schepaschenko, Olga Danylo, Martina Dürauer, Hedwig Bartl, Florian Hofhansl, Roman Zadorozhniuk, Maksym Burianchuk, Flavius Sirbu, Brigitte Magori, Kateryna Blyshchyk, Volodymyr Blyshchyk, Ahmed Harb Rabia, Chandra Kant Pawe, Yuan-Fong Su, Merajuddin Ahmed, Kripal Panging, Oleksandr Melnyk, Olesia Vasylyshyn, Roman Vasylyshyn, Andrii Bilous, Svitlana Bilous, Krishna Das, Reinhard Prestele, Ana Pérez-Hoyos, Khangsembou Bungnamei, Andrii Lashchenko, Maryna Lakyda, Ivan Lakyda, Oleksandr Serediuk, Galyna Domashovets, Yuriy Yurchuk, Michèle Koper, and Steffen Fritz. Drivers of tropical forest loss between 2008 and 2019. *Scientific Data*, 9(1):146, April 2022.

[47] Yating Li, Zhenzi Wu, Xiao Xu, Hui Fan, Xiaojia Tong, and Jiang Liu. Forest disturbances and the attribution derived from yearly Landsat time series over 1990–2020 in the Hengduan Mountains Region of Southwest China. *Forest Ecosystems*, 8(1):73, November 2021.

[48] Pablo A. López-Bedoya, Mauricio Bohada-Murillo, María Camila Ángel Vallejo, Livia Dorneles Audino, Adrian L. V. Davis, Geoff Gurr, and Jorge Ari Noriega. Primary forest loss and degradation reduces biodiversity and ecosystem functioning: A global meta-analysis using dung beetles as an indicator taxon. *Journal of Applied Ecology*, 59(6):1572–1585, 2022. _eprint: https://onlinelibrary.wiley.com/doi/pdf/10.1111/1365-2664.14167.

[49] Robert N. Masolele, Diego Marcos, Veronique De Sy, Itohan-Osa Abu, Jan Verbesselt, Johannes Reiche, and Martin Herold. Mapping the diversity of land uses following deforestation across Africa. *Scientific Reports*, 14(1):1681, January 2024.

[50] Victor Maus, Stefan Giljum, Dieison M. Da Silva, Jakob Gutschlhofer, Robson P.

Da Rosa, Sebastian Luckeneder, Sidnei L. B. Gass, Mirko Lieber, and Ian McCallum. An update on global mining land use. *Scientific Data*, 9(1):433, July 2022.

[51] Paulo J. Murillo-Sandoval, Thomas Hilker, Meg A. Krawchuk, and Jamon Van Den Hoek. Detecting and Attributing Drivers of Forest Disturbance in the Colombian Andes Using Landsat Time-Series. *Forests*, 9(5):269, May 2018. Number: 5 Publisher: Multidisciplinary Digital Publishing Institute.

[52] Mohsen Nabil, Miao Zhang, Bingfang Wu, Jose Bofana, and Abdelrazek Elnashar. Constructing a 30m African Cropland Layer for 2016 by Integrating Multiple Remote sensing, crowdsourced, and Auxiliary Datasets. *Big Earth Data*, 6(1):54–76, January 2022.

[53] Trung H. Nguyen, Simon D. Jones, Mariela Soto-Berelov, Andrew Haywood, and Samuel Hislop. A spatial and temporal analysis of forest dynamics using Landsat time-series. *Remote Sensing of Environment*, 217:461–475, November 2018.

[54] Julian Oeser, Dirk Pflugmacher, Cornelius Senf, Marco Heurich, and Patrick Hostert. Using Intra-Annual Landsat Time Series for Attributing Forest Disturbance Agents in Central Europe. *Forests*, 8(7):251, July 2017. Number: 7 Publisher: Multidisciplinary Digital Publishing Institute.

[55] Pontus Olofsson, Giles M. Foody, Martin Herold, Stephen V. Stehman, Curtis E. Woodcock, and Michael A. Wulder. Good practices for estimating area and assessing accuracy of land change. *Remote Sensing of Environment*, 148:42–57, May 2014.

[56] Diana Parker, Anna Tosiani, Muhammad Yazid, Inggit L. Sari, Tatik Kartika, Kustiyo, Rizky Firmansyah, Zuraidah Said, Arief Wijaya, Peter Potapov, Alexandra Tyukavina, Stephen V. Stehman, Viviana Zalles, Amy Pickens, Jeffrey Pickering, Svetlana Turubanova, and Matthew C. Hansen. Land in limbo: Nearly one third of Indonesia's cleared old-growth forests left idle. *Proceedings of the National Academy of Sciences*, 121(28):e2318029121, July 2024. Publisher: Proceedings of the National Academy of Sciences.

[57] Valerie J. Pasquarella, Christopher F. Brown, Wanda Czerwinski, and William J. Rucklidge. Comprehensive quality assessment of optical satellite imagery using weakly supervised video learning. In *2023 IEEE/CVF Conference on Computer Vision and Pattern Recognition Workshops (CVPRW)*, pages 2125–2135, Vancouver, BC, Canada, June 2023. IEEE.

[58] Timothy R. H. Pearson, Sandra Brown, Lara Murray, and Gabriel Sidman. Greenhouse gas emissions from tropical forest degradation: an underestimated source. *Carbon Balance and Management*, 12(1):3, February 2017.

[59] Jan Pišl, Marc Rußwurm, Lloyd Haydn Hughes, Gaston Lenczner, Linda See, Jan Dirk Wegner, and Devis Tuia. Mapping drivers of tropical forest loss with satellite image time series and machine learning. *Environmental Research Letters*, 19(6):064053, June 2024.

[60] Peter Potapov, Matthew C. Hansen, Amy Pickens, Andres Hernandez-Serna, Alexandra Tyukavina, Svetlana Turubanova, Viviana Zalles, Xinyuan Li, Ahmad

Khan, Fred Stolle, Nancy Harris, Xiao-Peng Song, Antoine Baggett, Indrani Kommareddy, and Anil Kommareddy. The Global 2000-2020 Land Cover and Land Use Change Dataset Derived From the Landsat Archive: First Results. *Frontiers in Remote Sensing*, 3:856903, April 2022.

[61] Anton Raichuk, Michelle Sims, Radost Stanimirova, and Maxim Neumann. Lightweight geospatial models for global deforestation attribution. In *NeurIPS 2024 Workshop on Tackling Climate Change with Machine Learning (CCAI)*, Vancouver, BC, Canada, December 2024.

[62] Neel Ramachandran, Jeremy Irvin, Hao Sheng, Sonja Johnson-Yu, Kyle Story, Rose Rustowicz, Andrew Y. Ng, and Kemen Austin. Automatic deforestation driver attribution using deep learning on satellite imagery. *Global Environmental Change*, 86:102843, May 2024.

[63] Adams C. Murrieta R. S. Ribeiro Filho, A. A. The impacts of shifting cultivation on tropical forest soil: a review. *Boletim Do Museu Paraense Emílio Goeldi. Ciências Humanas*, 8:693–727, 2013.

[64] Jessica Richter, Elizabeth Goldman, Nancy Harris, David Gibbs, Melissa Rose, Suzanne Peyer, Sarah Richardson, and Hemalatha Velappan. Spatial Database of Planted Trees (SDPT Version 2.0). *World Resources Institute*, March 2024.

[65] Daniel Rondinelli Roquetti, Simone Athayde, José Silva-Lugo, and Evandro Mateus Moretto. Amazon communities displaced by hydroelectric dams: Implications for environmental changes and householdś livelihood. *Global Environmental Change*, 89:102933, December 2024.

[66] Marcello Schiavina, Sergio Freire, Carioli, Alessandra, and MacManus, Kytt. *GHS-POP R2023A - GHS population grid multitemporal (1975-2030)*. European Commission, Joint Research Centre (JRC), 2023.

[67] Julius Sebald, Cornelius Senf, and Rupert Seidl. Human or natural? Landscape context improves the attribution of forest disturbances mapped from Landsat in Central Europe. *Remote Sensing of Environment*, 262:112502, September 2021.

[68] Cornelius Senf and Rupert Seidl. Storm and fire disturbances in Europe: Distribution and trends. *Global Change Biology*, 27(15):3605–3619, August 2021.

[69] Frances Seymour and Nancy L. Harris. Reducing tropical deforestation. *Science*, 365(6455):756–757, August 2019. Publisher: American Association for the Advancement of Science.

[70] Bart Slagter, Johannes Reiche, Diego Marcos, Adugna Mullissa, Etse Lossou, Marielos Peña-Claros, and Martin Herold. Monitoring direct drivers of small-scale tropical forest disturbance in near real-time with Sentinel-1 and -2 data. *Remote Sensing of Environment*, 295:113655, September 2023.

[71] Xiao-Peng Song, Matthew C. Hansen, Peter Potapov, Bernard Adusei, Jeffrey Pickering, Marcos Adami, Andre Lima, Viviana Zalles, Stephen V. Stehman, Carlos M. Di Bella, Maria C. Conde, Esteban J. Copati, Lucas B. Fernandes,

Andres Hernandez-Serna, Samuel M. Jantz, Amy H. Pickens, Svetlana Turubanova, and Alexandra Tyukavina. Massive soybean expansion in South America since 2000 and implications for conservation. *Nature Sustainability*, 4(9):784–792, June 2021.

[72] Stephen V. Stehman. Estimating area and map accuracy for stratified random sampling when the strata are different from the map classes. *International Journal of Remote Sensing*, 35(13):4923–4939, July 2014.

[73] Stephen V. Stehman and Giles M. Foody. Key issues in rigorous accuracy assessment of land cover products. *Remote Sensing of Environment*, 231:111199, September 2019.

[74] Christian Szegedy, Vincent Vanhoucke, Sergey Ioffe, Jon Shlens, and Zbigniew Wojna. Rethinking the inception architecture for computer vision. In *Proceedings of the IEEE conference on computer vision and pattern recognition*, pages 2818–2826, 2016.

[75] Liang Tang and Tim T. Werner. Global mining footprint mapped from high-resolution satellite imagery. *Communications Earth and Environment*, 4(1):1–12, April 2023.

[76] Prasad S. Thenkabail, Teluguntla, Pardhasaradhi G., Xiong, Jun, Oliphant, Adam, Congalton, Russell G., Ozdogan, Mutlu, Gumma, Murali K., Tilton, James C., Giri, Chandra, Milesi, Cristina, Phalke, Aparna, Massey, Richard, Yadav, Kamini, Temuulen Sankey, Ying Zhong, Itiya Aneece, and Daniel Foley. Global Cropland-Extent Product at 30-m Resolution (GCEP30) Derived from Landsat Satellite Time-Series Data for the Year 2015 Using Multiple Machine-Learning Algorithms on Google Earth Engine Cloud. Professional Paper, U.S. Geological Survey, 2021. Series: Professional Paper.

[77] A. Tyukavina, A. Baccini, M. C. Hansen, P. V. Potapov, S. V. Stehman, R. A. Houghton, A. M. Krylov, S. Turubanova, and S. J. Goetz. Aboveground carbon loss in natural and managed tropical forests from 2000 to 2012. *Environmental Research Letters*, 10(7):074002, July 2015.

[78] Alexandra Tyukavina, Matthew C. Hansen, Peter Potapov, Diana Parker, Chima Okpa, Stephen V. Stehman, Indrani Kommareddy, and Svetlana Turubanova. Congo Basin forest loss dominated by increasing smallholder clearing. *Science Advances*, 4(11):eaat2993, November 2018.

[79] Alexandra Tyukavina, Matthew C. Hansen, Peter V. Potapov, Stephen V. Stehman, Kevin Smith-Rodriguez, Chima Okpa, and Ricardo Aguilar. Types and rates of forest disturbance in brazilian legal amazon, 2000–2013. *Science Advances*, 3(4):e1601047, April 2017.

[80] Alexandra Tyukavina, Peter Potapov, Matthew C. Hansen, Amy H. Pickens, Stephen V. Stehman, Svetlana Turubanova, Diana Parker, Viviana Zalles, André Lima, Indrani Kommareddy, Xiao-Peng Song, Lei Wang, and Nancy Harris. Global Trends of Forest Loss Due to Fire From 2001 to 2019. *Frontiers in Remote Sensing*, 3:825190, March 2022.

[81] Nathalie van Vliet, Ole Mertz, Andreas Heinimann, Tobias Langanke, Unai Pascual, Birgit Schmook, Cristina Adams, Dietrich Schmidt-Vogt, Peter Messerli, Stephen Leisz, Jean-Christophe Castella, Lars Jørgensen, Torben Birch-Thomsen, Cornelia Hett, Thilde Bech-Bruun, Amy Ickowitz, Kim Chi Vu, Kono Yasuyuki, Jefferson Fox, Christine Padoch, Wolfram Dressler, and Alan D. Ziegler. Trends, drivers and impacts of changes in swidden cultivation in tropical forest-agriculture frontiers: A global assessment. *Global Environmental Change*, 22(2):418–429, May 2012.

[82] Yunxia Wang, Peter M. Hollingsworth, Deli Zhai, Christopher D. West, Jonathan M. H. Green, Huafang Chen, Kaspar Hurni, Yufang Su, Eleanor Warren-Thomas, Jianchu Xu, and Antje Ahrends. High-resolution maps show that rubber causes substantial deforestation. *Nature*, 623(7986):340–346, November 2023.

[83] Rebecca B. Wayman and Hugh D. Safford. Recent bark beetle outbreaks influence wildfire severity in mixed-conifer forests of the sierra nevada, california, usa. *Ecological Applications*, 31(3):e02287, 2021.

[84] Mikaela Weisse and Peter Potapov. Assessing trends in tree cover loss over 20 years of data, April 2021.

[85] D. Zanaga, R. Van De Kerchove, D. Daems, W. De Keersmaecker, C. Brockmann, G. Kirches, J. Wevers, O. Cartus, M. Santoro, S. Fritz, M. Lesiv, M. Herold, N.-E. Tsendbazar, P. Xu, F. Ramoino, and O. Arino. ESA WorldCover 10 m 2021 v200, October 2022.

[86] Yingtong Zhang, Curtis E. Woodcock, Shijuan Chen, Jonathan A. Wang, Damien Sulla-Menashe, Zhenpeng Zuo, Pontus Olofsson, Yetianjian Wang, and Mark A. Friedl. Mapping causal agents of disturbance in boreal and arctic ecosystems of North America using time series of Landsat data. *Remote Sensing of Environment*, 272:112935, April 2022.

[87] Alan D. Ziegler, Thilde B. Bruun, Maite Guardiola-Claramonte, Thomas W. Giambelluca, Deborah Lawrence, and Nguyen Thanh Lam. Environmental consequences of the demise in swidden cultivation in montane mainland southeast asia: Hydrology and geomorphology. *Human Ecology*, 37(3):361–373, June 2009.

[88] Guy Ziv, Eric Baran, So Nam, Ignacio Rodríguez-Iturbe, and Simon A. Levin. Trading-off fish biodiversity, food security, and hydropower in the mekong river basin. *Proceedings of the National Academy of Sciences*, 109(15):5609–5614, April 2012.

Supplementary Information
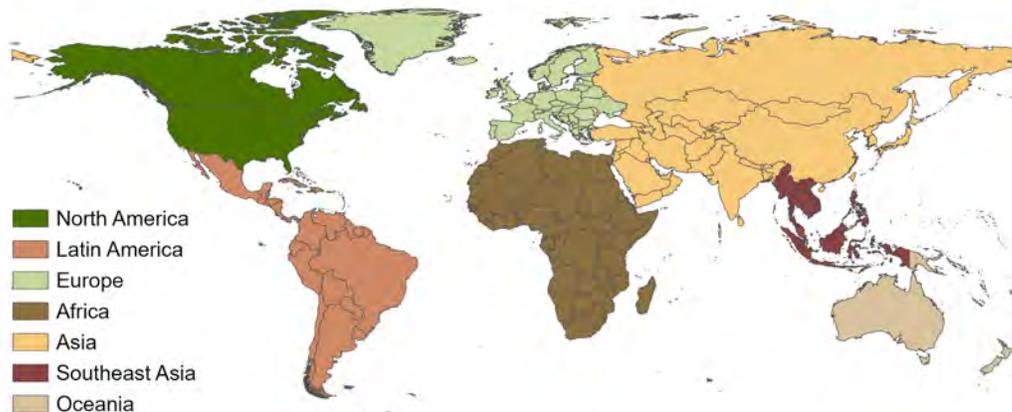
Figure S1. Geographic boundaries used for regional reporting units

S1. Training and validation data collection

An initial set of training samples were generated using a global stratified random sample. Samples were collected from the 0.01 degree grid (approximately 1 km at the equator) overlaid with tree cover loss data from the GFC product v.10 [26]. To avoid sampling noise, we subset the grid cells to those where tree cover loss makes up at least 0.5%. The stratification was based on the seven driver classes and was aided by ancillary data layers. The stratified sample was complemented by an additional smaller random sample to ensure full coverage and potentially capture dynamics not represented by the ancillary data used for stratification.

Training data were interpreted by a team of nine trained image analysts using the drivers of forest loss definitions (Table 1 in main text) and a suite of online tools, accessed through the Google Earth Engine API [25]. Training data were assigned by region to each analyst. All analysts received the same training to ensure consistency in their interpretation, followed by a practice set that was discussed as a group so that analysts improved the quality of their interpretations and understood the dynamics of each driver in each region.

Image analysts interpreted drivers on-screen using a combination of high-resolution imagery from Google Earth Pro and Esri Wayback, annual composites from Landsat Collection 1 (C1) and Sentinel-2, and biannual Planet composites provided by Norway's International Climate and Forests Initiative (NICFI) Satellite Data Program. Image analysts also referred to time series of spectral reflectance (shortwave infrared (SWIR1) band), indices (Normalized Difference Vegetation Index (NDVI), Normalized Burn Ratio

(NBR)), and Tasseled Cap transformations (wetness, brightness) derived from Landsat C1. Lastly, image analysts used contextual layers such a tree cover loss due to fire [80] and MODIS burned area (MCD64A1.061, [24]), along with land cover and land use products (Table S3). Contextual layers were only used as corroborating evidence for interpretations made using satellite imagery and time series and were not used as the sole basis for interpretation, given that the datasets contain errors of omission and commission. Where available analysts also used Google Earth photos and Places tags along with Street View as a source of contextual information.

The 1 km grid cells containing tree cover loss according to [26] (updated through 2022) served as the basic unit of interpretation. For each grid cell (plot), analysts collected information on the primary driver of loss (greater than 50% of the loss within the plot), secondary driver of loss, and their confidence in assigning each label. Confidence was assigned as *low*, *medium*, or *high*. We collected additional levels of detail that were not used in the analysis: 1) for hard commodities we differentiated between *mining* and *energy*, 2) for permanent agriculture we differentiated between *tree crop management* and *agriculture*. Tree crop management was defined as loss associated with pruning, replanting, or other management activities within orchards or tree crop plantations that were already established as of the year 2000 (or before the year of loss), and agriculture was defined as loss of tree cover for new agricultural activities.

Each plot was reviewed for quality by a duo of senior analysts with domain expertise. If necessary, the plot was reinterpreted in consultation between the senior analysts. Plots that remained low confidence after the quality review were dropped from the analysis but are provided in the Zenodo data repository (see section 7 of main text). Units remained labeled low confidence in cases where there was no high-resolution imagery available and team members had no reliable alternative way to assign a driver of forest loss. Lastly, we had a "noise" category that was used when the tree cover loss data by [26] indicated loss but upon interpretation it turned out to be a false positive with no actual loss on the ground (e.g., due to cloud or sensor issues, shadows, misclassification of wetland water fluctuations etc.). In some cases, shrubland loss was detected as tree cover loss by [26]. For the purposes of training data collection, shrubland loss (such as shrubland fires or conversion, or the pruning of shrubby crops such as grape vines, coffee and tea) were labeled according to the corresponding driver of loss. All of these transitions represent the loss of woody vegetation, sometimes at heights near the 5 m threshold. In addition to the quality assessment outlined above, the training plots were reviewed for clerical errors and compiled into a unique database for each region. This resulted in a total of 4,820 plots globally.

We collected additional training plots via an active learning workflow to improve the initial drivers of forest loss classification because the initial training plots were geographically incomplete and did not adequately represent all forest loss dynamics globally. We took an additional sample of 2,433 plots that were identified in three ways: 1) visual inspection of the maps to identify large scale misclassification, 2) plots where the first and second most likely class had a probability margin (difference between

probabilities) of 1% or less, and 3) plots for which the classification of the two models we were initially testing disagreed (a random forest model and a ResNet model– see subsection 2.4 in main text).

The initial training dataset and active learning dataset combined resulted in 7,786 plots, of which 831 (11%) were removed due to low confidence (7%) and noise (4%). The resulting final training dataset used in model development had 6,955 plots (Figure S2, Table S1), the majority of which had high confidence (80%). Nearly a quarter (22%) had a secondary driver in addition to a primary driver.

An additional stratified random sample of 3,574 1 km plots (Figure S3) was used to estimate the accuracy of the final classification map. We used the same interpretation protocol for the validation and training data collection with two differences: 1) we used monthly Sentinel-2 and Landsat composites as opposed to annual composites, and 2) we used Landsat C2 as opposed to C1, due to the deprecation of C1 in Google Earth Engine and the improvements in processing for C2. Validation plots were identified and collected independently of training plots following the best practices outlined in [55] and [73]. We stratified our accuracy assessment based on seven regions and seven driver classes for a total of 49 strata. Sample sizes per strata were derived using an initial map version and an optimal sample allocation based on guidance in [55]. We targeted standard errors from 0.05% to 0.2% for rare and common classes respectively, and 95% confidence interval. Plots were allocated to strata using a minimum sample size of 40 for rare classes, and the rest were allocated proportionally as recommended in [55]. The sample size was a compromise between practical considerations (e.g., resources) and precision.
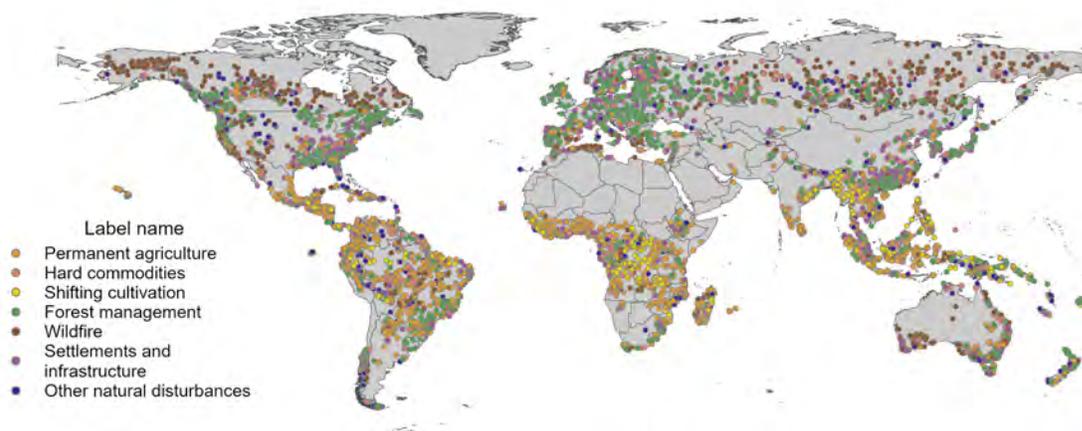
Figure S2. Global training plots

Table S1. Number of training plots per region and driver class. LaAm stands for Latin America, NoAm stands for North America, SEAsia stands for Southeast Asia

Driver category	Africa	Asia	Oceania	Europe	LaAm	NoAm	SEAsia	Total
Permanent agriculture	487	200	115	66	693	114	311	1986 (28.6%)
Hard commodities	67	143	36	51	84	69	59	509 (7.3%)
Shifting cultivation	243	48	64	0	91	0	118	564 (8.1%)
Forest management	92	423	193	373	236	290	95	1702 (24.5%)
Wildfire	113	324	162	91	103	270	50	1113 (16.0%)
Settlements and infrastr.	80	154	100	99	80	111	41	665 (9.6%)
Other natural disturbances	35	86	61	21	105	74	34	416 (6.0%)
Total	1117	1378	731	701	1392	928	708	6955
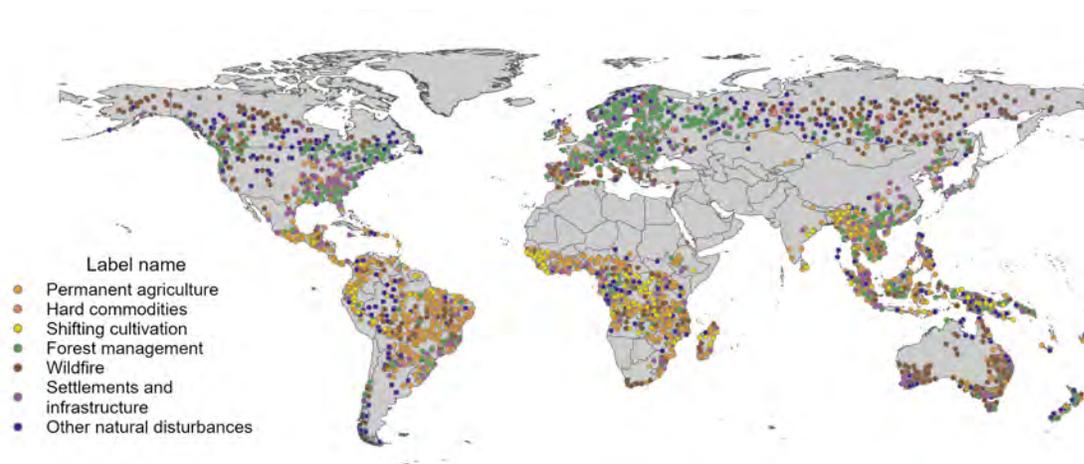
Figure S3. Global validation plots

Table S2. Number of validation plots per region and driver class. LaAm stands for Latin America, NoAm stands for North America, SEAsia stands for Southeast Asia. Number of non-noise plots are shown first along with total number of plots in parenthesis

Driver category	Africa	Asia	Oceania	Europe	LaAm	NoAm	SEAsia
Permanent agriculture	232 (236)	46 (54)	91 (105)	31 (35)	351 (372)	37 (44)	207 (210)
Hard commodities	9 (9)	38 (38)	13 (13)	9 (10)	17 (17)	13 (13)	27 (27)
Shifting cultivation	126 (126)	28 (28)	51 (51)	0 (0)	41 (41)	0 (0)	50 (50)
Forest management	27 (27)	132 (132)	86 (88)	262 (264)	38 (38)	155 (155)	68 (68)
Wildfire	95 (96)	134 (136)	193 (194)	37 (37)	70 (70)	84 (84)	45 (45)
Settlements and infrastr.	35 (35)	30 (30)	35 (35)	42 (42)	34 (34)	50 (50)	30 (30)
Other natural disturbances	28 (44)	72 (81)	58 (69)	31 (37)	42 (50)	77 (86)	37 (38)

Table S3. Description and sources for contextual data layers used in visual interpretation and training data collection, Contextual layers were only used as corroborating evidence for interpretations made using satellite imagery and time series and were not used as the sole basis for interpretation, given that the datasets contain errors of omission and commission.

Name	Theme	Date of Content	Resolution	Source
Global forest loss due to fire	Fire	2001 to 2022	30 m	[80]
MODIS burned area (MCD64A1.061)	Fire	2001 to 2022	500 m	[24]
IIASA mining	Mining	2000 to 2019	30 arc-second	[50]
Global Land Cover and Land Use Change: forest extent and height	Forest	2000 and 2020	30 m	[60]
Global Land Cover and Land Use Change: built-up	Urban	2000 to 2020	30 m	[60]
ESA WorldCover	Land Cover	2020 and 2021	10 m	[85]
Spatial Database of Planted Trees v2	Plantation	Varies 2015	Varies	[64]
USGS Global Cropland Extent Product at 30m Resolution (GCEP30)	Croplands	2015	30 m	[76]
Global Land Cover and Land Use Change: croplands	Croplands	2000 to 2019	30 m	[60]
Digital Earth Africa's cropland extent map Africa	Croplands	2019	10 m	[1]
Ensemble Source Africa Cropland Mask	Croplands	2016	30 m	[52]
ETH/Ecovision Cocoa Map	Tree crops	2019 to 2021	10 m	[38]
Laos shifting cultivation	Shifting cultivation	1991 to 2020	30 m	[11]
Southeast Asia rubber extent	Tree crops	2021	10 m	[82]
Africa follow on land use	Land Use	2020	5 m	[49]

S2. Specifications and pre-processing of model input data

The basis of this model and a core input is the GFC product v1.10 [26], which includes the year of tree cover loss along with first and last Landsat 7 cloud-free composite, updated through 2022, at 1 arc second (approximately 30m at the equator). The first composite is from the first available year, circa 2000. The last image composite is from 2022 or the closest year with cloud free data. The reference composite imagery are median observations from a set of quality assessed growing season observations in four spectral bands: red, near-infrared (NIR), and two short-wavelength infrared bands (SWIR1 and SWIR2). Since our analysis is based on the Global Forest Change [26] tree cover loss data, it is subject to its limitations (see subsection 4.4 in main text).

The model included three years of Sentinel-2 data from 2018, 2020, and 2022, representing the later years of the time period included in the model. We tested the inclusion of all available years of Sentinel-2 data and various combinations of years at regular time intervals, and selected this combination based on evaluating performance benefits versus computational costs. Sentinel-2 data were further processed by filtering out cloudy areas using the Cloud Score+ with a default clear threshold below 60% [57]. We tested both top-of-atmosphere (L1C) and processed surface reflectance (L2A); the results were similar, and we selected to use L1C, because it has a larger temporal range of data availability within Google Earth Engine (data available in 2015 vs. 2017 for L2A). Sentinel composites are created by taking the mean value of the 3-month peak summer period, corresponding to June-August for the northern hemisphere and December-February for the southern hemisphere. We used the following Sentinel-2 bands: [B3, B4, B5, B7, B12], which have 10 or 20 m nominal resolution.

In addition to satellite observations, we included ancillary biophysical and population datasets as predictor variables such as tree cover loss due to fire [80], elevation data [28], the Global Human Settlement Layer (GHSL) Global Population Surfaces [66], Dynamic World v1 [9], and a mining dataset that we created by combining three publicly available datasets [50, 17, 75]. Elevation and topographical variables have been found in previous studies to be an important predictor variable in forest disturbance attribution, as some types of disturbances may occur more frequently at higher elevations [40, 54, 67]. Data on fires and population distribution has relevance for our driver classes and similar variables have been used in prior studies [13]. The tree cover loss from fires data [80] has a particular advantage over other fire datasets, such as MODIS-based burned area products [24], in that loss due to fire is defined in a similar manner as our wildfire class. We converted the tree cover loss due to fire data to a binary raster with values of 0 (not fire) and 1 (fire), including medium to high levels of certainty in the fire category [80]. These data are available at 1 arc second (approximately 30 m at the equator), and updated through 2022. Elevation data were obtained from the Copernicus GLO 30 resolution Digital Elevation Model with forest and building removed (FABDEM). The data are available at 1 arc second (approximately 30 m at the equator) for the globe [28]. We used the elevation, slope, and aspect. Global population data were obtained

from the GHSL Global Population Surfaces, which depicts the spatial distribution of residential populations derived from CIESIN GPWv4.11 and disaggregated from census and administrative units to grids at a resolution of 100 m [66]. We use GHSL estimates for the years 1995, 2000, 2005, 2010, 2015, 2020, and 2025 (projected). We used the *grass, crops,* and *shrub/scrub* class probabilities from the Dynamic World dataset [9] for the years 2016, 2019, and 2022. We took the mean class probability for each of these three classes over each year. Similar to Sentinel-2, we initially tested the inclusion of all class probabilities and all available years of Dynamic World and various combinations of years at regular time intervals, and found that this class and year combination yielded the best performance benefits across a range of accuracy metrics. We created the mining dataset by combining (via union) three separate datasets mapping the location of mining sites [50, 75] and alluvial mining [17] worldwide. All three datasets were created through manual delineation of polygons using satellite imagery. We converted these datasets to a binary raster (0/1) corresponding to the presence of mining sites. Lastly, we included latitude and longitude as predictor variables and created a one hot encoding for the seven regions, a binary numerical value (0/1) that corresponded to each region.

All input data were resampled to a common spatial resolution of 0.5 arc seconds, or approximately 15 m at the equator, which we found provided a good trade-off between accuracy and computational costs. Although inference maps were generated at 1 km, we used a larger context window (approximately 1.5 km) for the input image, as we found that including more contextual information improved the training accuracy and reduced noise in the resulting inference maps. These dataset generation steps were conducted in Google Earth Engine [25] using the GeeFlow package, resulting in model input data as presented in Table 2 of the main text.

To create inputs for model training and evaluation, additional operations were performed. All non-binary data layers were normalized to have 0 mean and 1 standard deviation. Pixels with no valid data were assigned a value of 0 post normalization. The temporal dimension in multi-temporal tensors was moved to the channels dimension, and all input data sources were stacked together in the channels dimension, to form 112 x 112 x 59 (height x width x channels) input tensors (including 13 GFC channels, 15 Sentinel-2, 7 GHSL, 1 fires, 1 mining, 9 Dynamic World, and 3 channels from spherical encoding of latitude and longitude, and 7 channels for one-hot region encoding). During training, the input tensors were randomly augmented using random rotations and flipping as well as cyclical shifts—a standard approach in deep learning to increase the diversity of training data. This allowed for the training data to appear slightly different at each epoch iteration of the model and to avoid overfitting (memorization of example specifics).

S3. Model training and ensembling

To tune the model and optimize the parameters, we used a 5-fold cross-validation. The model was trained for 10 epochs (that is, each example is seen 10 times by the model, slightly randomly augmented each time) with gradient descent using the Adam optimizer

Table S4. Parameters for the best model configuration (deviating from default) and training configuration.

Name	Value
model depth	2
model width	256
model stem conv kernel size	(1, 1)
model stem conv stride	(1, 1)
model stem pool kernel size	(6, 6)
model stem pool stride	(2, 2)
optimizer	Adam
base learning rate	0.01
weight decay	0.00003
gradient clip norm	1.0
batch size	128
training epochs	10
learning rate schedule	cosine decay
warmup	2 epochs
loss	softmax cross-entropy

with weight decay [41].

For robust evaluation, we used 20 random seeds to initialize the model weights and for training data random augmentation, resulting in total in 100 trained models (5 folds x 20 random seeds). For a full list of the tuned training parameters for the best model configurations, see Table S4. We also tested training a separate model for each region versus training one global model, and found that we achieved higher performance with a global model.

Since we had a relatively small number of examples for a deep learning approach, we ensemble a set of trained models to reduce model uncertainty [8]. Model ensembling delivers the best results if the underlying models or training schemes are slightly different. Therefore we constructed an ensemble by varying model depth and width (2x deeper / broader), number of training epochs (10, 20, 40 epochs), random seeds for model weight initialization, etc. For each 5-folds model training (training on 4 folds, evaluating on the 5th), we selected the best two models based on the evaluation fold to be kept in the ensemble. Additionally, we used the technique of "label smoothing" for some models in the ensemble, which makes the training more robust against potential errors and uncertainties in the training data [74].

Table S5: Regional class accuracies and driver proportions. PA stands for producer's accuracy, UA stands for user's accuracy, SE stands for standard error, CI stands for 95% confidence interval.

Region	Class	UA	UA SE	UA CI	PA	PA SE	PA CI
North America	Perm ag	81.1	12.8	25.1	78.9	12.8	25.1
North America	Hard com	56.5	23.4	45.9	2.3	2.1	4.2
North America	Forest man	91.5	2.7	5.4	96.3	2.3	4.6
North America	Wildfires	96.0	2.7	5.4	97.6	2.0	3.9
North America	Settle	68.8	14.1	27.7	42.1	12.2	23.9
North America	Nat dist	75.8	10.1	19.8	55.2	15.4	30.2
Europe	Perm ag	86.4	7.1	13.9	32.2	13.0	25.4
Europe	Hard com	47.1	23.8	46.7	34.0	19.1	37.4
Europe	Forest man	95.1	1.6	3.2	99.1	0.5	1.0
Europe	Wildfires	94.8	3.0	5.9	91.2	5.6	10.9
Europe	Settle	51.6	18.6	36.4	39.7	17.8	34.8
Europe	Nat dist	18.4	16.0	31.3	7.4	4.3	8.5
Africa	Perm ag	86.8	2.9	5.7	94.8	2.5	4.9
Africa	Hard com	98.2	2.0	3.9	55.3	20.7	40.5
Africa	Shift cult	88.8	3.6	7.1	89.6	3.7	7.2
Africa	Forest man	83.3	8.8	17.2	85.3	8.8	17.2
Africa	Wildfires	94.4	3.4	6.6	29.6	7.4	14.4
Africa	Settle	84.4	10.4	20.4	73.3	16.1	31.6
Africa	Nat dist	57.7	20.5	40.1	25.9	12.6	24.7
Asia	Perm ag	84.2	8.0	15.7	52.0	13.3	26.0
Asia	Hard com	96.5	2.5	4.9	50.9	11.0	21.6
Asia	Shift cult	74.9	11.5	22.6	81.2	15.0	29.3
Asia	Forest man	87.0	3.3	6.4	97.8	1.0	1.9
Asia	Wildfires	98.2	1.3	2.6	99.3	0.3	0.6
Asia	Settle	66.6	10.3	20.2	81.0	8.2	16.0
Asia	Nat dist	88.9	6.3	12.3	49.1	15.5	30.3
Southeast Asia	Perm ag	87.6	2.8	5.5	90.1	2.8	5.4
Southeast Asia	Hard com	82.6	11.4	22.3	82.2	8.1	15.9
Southeast Asia	Shift cult	61.3	8.5	16.7	70.6	9.0	17.6
Southeast Asia	Forest man	88.9	7.5	14.8	75.3	7.2	14.2
Southeast Asia	Wildfires	71.0	14.1	27.6	73.9	13.0	25.5
Southeast Asia	Settle	58.0	20.2	39.6	77.3	10.9	21.4
Southeast Asia	Nat dist	30.4	12.7	24.9	10.4	4.9	9.7
Oceania	Perm ag	71.2	10.0	19.7	65.0	10.4	20.4
Oceania	Hard com	87.7	8.7	17.1	91.2	7.5	14.7

Table S5: Regional class accuracies and driver proportions. PA stands for producer's accuracy, UA stands for user's accuracy, SE stands for standard error, CI stands for 95% confidence interval.

Region	Class	UA	UA SE	UA CI	PA	PA SE	PA CI
Oceania	Shift cult	62.2	12.2	24.0	83.0	5.6	10.9
Oceania	Forest man	91.5	2.6	5.0	89.7	4.5	8.9
Oceania	Wildfires	96.2	1.8	3.5	95.6	1.8	3.6
Oceania	Settle	67.2	9.4	18.5	80.2	8.2	16.1
Oceania	Nat dist	62.8	9.1	17.8	66.8	7.2	14.2
Latin America	Perm ag	93.6	1.4	2.8	96.6	1.0	1.9
Latin America	Hard com	99.1	1.0	2.0	83.0	11.2	22.0
Latin America	Shift cult	55.1	11.8	23.1	49.2	10.8	21.1
Latin America	Forest man	82.9	7.0	13.7	97.6	1.2	2.4
Latin America	Wildfires	98.6	1.2	2.3	71.5	8.3	16.3
Latin America	Settle	72.9	14.3	28.1	83.8	7.5	14.6
Latin America	Nat dist	42.3	12.5	24.4	49.0	13.3	26.0
Global	Perm ag	90.3	1.2	2.3	92.8	1.1	2.1
Global	Hard com	92.2	3.9	7.6	60.3	8.9	17.5
Global	Shift cult	78.5	3.3	6.5	80.6	3.4	6.7
Global	Forest man	89.6	1.7	3.3	95.0	1.1	2.2
Global	Wildfires	96.9	1.1	2.1	92.8	1.3	2.6
Global	Settle	67.1	6.4	12.5	61.8	7.2	14.2
Global	Nat dist	67.8	5.9	11.6	45.1	7.5	14.7

S4. Discussion of Limitations

There are several important limitations to this work. First, our model and resulting maps are limited in scope to classifying the driver of forest loss as mapped by the Global Forest Change product [26], and therefore the detection and quantification of loss is subject to the accuracy of that product. Known limitations include, but are not limited to, algorithm adjustments that cause inconsistencies in the data over time [84], underestimation of tree cover loss in the early 2000s and overestimation of loss in the 2010s in the Congo Basin [78] and Brazilian Legal Amazon [79], underestimation of tree cover loss in forest ecosystems with low canopy cover [77], and misclassification of shrubland/grassland loss, cropland dynamics, or wetland dynamics as tree cover loss observed by the authors of this study through training and validation data collection.

Tree cover loss as defined by [26] includes disturbances in both natural and planted forests. In this study, we do not distinguish between the loss of natural forest (including primary or secondary forest) and planted forest (including plantations, agroforestry systems, or other planted trees). While we consider tree cover loss associated with the permanent agriculture, hard commodities, and settlements and infrastructure classes to

represent a close approximation of deforestation, users should note that these classes do not always represent the conversion of *natural* forests to other land uses. For example, the permanent agriculture class includes the replacement of existing tree crops established before 2000, in addition to the conversion of natural forest to tree crops or other forms of agriculture. However, the replacement of existing tree crops likely represents a relatively small proportion of the total area of the permanent agriculture driver – 14% of training plots and 11% of validation plots within the permanent agriculture class contained the tree crop management tag (see section S1), indicating loss of existing tree crops. This percentage increases for regions with a longer history of tree crop establishment. Users should consider this when interpreting this driver for regions where tree crops were established prior to 2000, such as the Central Valley in California, United States and parts of peninsular Malaysia, for example. Similarly, replacement of natural forest with wood fiber plantations is not distinguished from routine harvesting within existing plantations established before 2000, as these are both included in the forest management class. Overlaying our drivers product with ancillary data on primary or natural forest extent to limit analysis to tree cover loss occurring within natural forest can address these limitations.

Our study includes salvage and sanitation logging in the forest management class, due to the challenges of disentangling natural disturbances from salvage logging when they occur in quick succession. This is particularly relevant in Europe, where salvage logging following natural disturbances, such as windthrow or bark beetle outbreaks, is common. Prior studies found that the increasing frequency of natural disturbances in Europe has led to increased harvest rates in recent years [67, 54]. Our data cannot separate harvest or logging in routine management cycles from logging in response to natural disturbances.

Finally, because we map the dominant driver of tree cover loss within each 1 km grid from 2001 to 2022, we do not disentangle different drivers that are co-located at scales smaller than 1 km. In some highly heterogeneous landscapes with mosaics of various land uses, particularly in the tropics, multiple drivers of forest loss can occur in close proximity. Future work should prioritize mapping drivers of forest loss at a higher temporal resolution (e.g., annually) and spatial resolution (e.g., 30 m pixel scale or disturbance scale) in order to understand the temporal sequence of co-located drivers at small spatial scales.